An Elastic Network Model Based on the Structure of the Red Blood Cell Membrane Skeleton

J. C. Hansen,* R. Skalak,*‡ S. Chien,* and A. Hoger*‡
*Department of Bioengineering, ‡Division of Mechanical Engineering, Department of Applied Mechanics and Engineering Science, University of California, San Diego, La Jolla, California 92093 USA

ABSTRACT A finite element network model has been developed to predict the macroscopic elastic shear modulus and the area expansion modulus of the red blood cell (RBC) membrane skeleton on the basis of its microstructure. The topological organization of connections between spectrin molecules is represented by the edges of a random Delaunay triangulation, and the elasticity of an individual spectrin molecule is represented by the spring constant, K, for a linear spring element. The model network is subjected to deformations by prescribing nodal displacements on the boundary. The positions of internal nodes are computed by the finite element program. The average response of the network is used to compute the shear modulus (μ) and area expansion modulus (κ) for the corresponding effective continuum. For networks with a moderate degree of randomness, this model predicts $\mu/K = 0.45$ and $\kappa/K = 0.90$ in small deformations. These results are consistent with previous computational models and experimental estimates of the ratio μ/κ. This model also predicts that the elastic moduli vary by 20% or more in networks with varying degrees of randomness. In large deformations, μ increases as a cubic function of the extension ratio λ_1, with $\mu/K = 0.62$ when $\lambda_1 = 1.5$.

INTRODUCTION

The mechanical properties of biological materials originate in structures that are assembled, controlled, and disassembled by cellular- and molecular-level processes. An understanding of the influence of these microstructures on macroscopic mechanical behavior is useful for the elucidation of the molecular basis of cell function in health and disease. (In this context, "macroscopic" refers to a length scale for which the mechanical contributions of discrete features within a material may be averaged and replaced by an equivalent continuum representation.) Continuum constitutive laws can be used to describe the macroscopic mechanical properties of such materials, but models that explicitly incorporate molecular structure are essential when relating macroscopic properties to discrete microscale features within a material. For most biological materials, the structural organization of molecular components is extremely complex, making it difficult to establish quantitative relationships between microstructure and mechanical function. The objective of our work is to explore this relationship in one type of biological microstructure: the red blood cell (RBC) membrane skeleton.

The RBC membrane skeleton is a flexible protein meshwork, composed mainly of spectrin, which reinforces the cytoplasmic face of the RBC membrane. The elasticity of the skeleton enables normal RBCs to undergo large extensional deformations while maintaining the structural integrity of the membrane. The general organization of the RBC membrane skeleton has been well characterized. The major protein components have been identified and sequenced, the interactions among these proteins have been studied, the membrane skeleton has been visualized with electron microscopy (EM) and atomic force microscopy (AFM), the mechanical properties of the membrane have been determined experimentally, and the membrane has been modeled as a continuum for purposes of mechanical engineering analysis.

Mature human RBCs lack nuclei and transcellular filaments, so the deformability of a RBC is a result of three factors (Chien, 1977): the ratio of membrane surface area to cell volume, the viscosity of the cytoplasm, and the deformability of the membrane. Membrane deformability may be characterized by three elastic parameters: the area expansion (bulk) modulus, κ_m; the shear modulus, μ_m; and the bending stiffness, B_m (see e.g., Evans and Skalak, 1980). The lipid bilayer strongly resists changes in area and therefore dominates the behavior of the membrane in both isotropic expansion and bending (Mohandas and Evans, 1994). The resistance of the red cell membrane to shear deformations is primarily attributable to the elasticity of the underlying skeleton (Evans, 1973; Mohandas et al., 1983). Both the shear modulus of the skeleton, μ, and the area expansion modulus of the skeleton, κ, affect the overall shear modulus of the membrane, μ_m, as measured by micropipette aspiration (Mohandas and Evans, 1994). Therefore, efforts to correlate mechanical properties with discrete structural features of the membrane have been focused on the elasticity of the skeleton.

The influence of skeletal microstructure on membrane mechanics has been documented by the significant changes in the membrane shear modulus that occur in genetic (e.g., Palek and Jarolim, 1993) and physiochemical (e.g., Deu-

Received for publication 26 June 1995 and in final form 26 September 1995.

Address reprint requests to Dr. Anne Hoger, Department of Applied Mechanics and Engineering Science, University of California, San Diego, La Jolla CA 92093-0411. Tel.: 619-534-2169; Fax: 619-534-7078; E-mail: ahoger@ucsd.edu.

0006-3495/96/01/146/21 $2.00

ticke et al., 1990) alterations of the RBC membrane skeleton. Although it is evident that there is a link between skeletal microstructure and membrane macroscopic properties, this relationship can only be explored explicitly by using mechanical models that are based on this microstructure. Because there is a substantial body of information available for the RBC membrane skeleton, it is possible to formulate and test a theory that describes the role of membrane microstructure in mechanical function.

THE RBC MEMBRANE SKELETON

The major proteins of the RBC membrane skeleton include spectrin, actin, protein 4.1, ankyrin, and the anion channel (band 3) (e.g., Shen, 1989; Chien and Sung, 1990; Bennett and Gilligan, 1993). A schematic drawing of the interactions among these proteins is shown in Fig. 1. The primary structural component of the RBC skeleton is spectrin, a highly extensible elastic molecule. A spectrin heterodimer is composed of one α subunit and one β subunit, which form an antiparallel pair of intertwined strands (Shen, 1989). Each strand is a triple-coiled coil of interlocking α helices and contains 18 to 20 homologous, nonidentical repeats of a 106-residue amino acid sequence (Speicher and Marchesi, 1984; Parry et al., 1992; Yan et al., 1993). The head ends of spectrin dimers (SpD) can self-associate to form tetramers (SpT), hexamers (SpH), and higher order oligomers, which coexist in a state of thermodynamic equilibrium (Ungewickell and Gratzer, 1978; Ralston, 1991). The relative proportions of the oligomeric forms of spectrin have been measured by biochemical analysis of spectrin

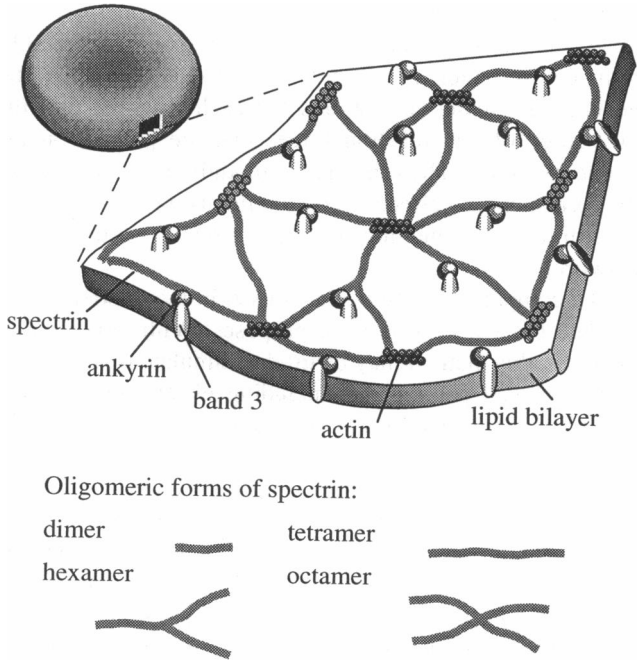

FIGURE 1 Arrangement of the major components of the RBC membrane skeleton.

membrane extracts (Liu et al., 1984), EM of fully spread, negatively stained skeletons (Liu et al., 1987), and EM of intact skeletons prepared by a quick-freeze, deep-etch, rotary replication (QFDERR) procedure (Ursitti et al., 1991; Ursitti and Wade, 1993; Ohno et al., 1994). Although EM images of fully spread skeletons seem to contain a very high fraction of tetramers with only 11% hexamers, the other methods mentioned above detect 14–40% hexamers, suggesting that higher-order oligomers may be disrupted by the process of spreading and negative staining (Ursitti and Wade, 1993). Recently, AFM has been used to visualize the cytoplasmic face of the RBC membrane (Miyamoto et al., 1993; Mikrut and MacDonald, 1994). These images are also suggestive of a relatively large fraction of hexamers in the native RBC membrane skeleton. Observations are expected to represent physiological conditions more closely when the skeleton remains attached to the lipid bilayer, as is the case for the QFDERR and AFM techniques.

At the end of the dimer opposite to that which is involved in spectrin self-association, spectrin binds to a junctional complex composed primarily of actin and protein 4.1 (see e.g., Gilligan and Bennett, 1993). Each junctional complex contains a single actin filament composed of ~12–13 monomers, which is believed to be constrained to this length by the actions of tropomyosin and tropomodulin (Ursitti and Fowler, 1994). Spectrin-actin interactions are considerably strengthened by the presence of protein 4.1 (Fowler and Taylor, 1980; Ohanian et al., 1984). The stoichiometry of spectrin and actin in junctional complexes is variable, with as few as three or as many as eight spectrin molecules joined to a single actin filament. The average number of spectrin molecules per junctional complex (Sp/JC) is between five and six in spread, negatively stained skeletons (Byers and Branton, 1985; Liu et al., 1987; Ursitti and Wade, 1993) and between four and five in skeletons prepared by the QFDERR technique (Ursitti and Wade, 1993).

Band 3 is a transmembrane protein that serves as a major site of skeletal attachment to the lipid bilayer. The flexible cytoplasmic domain of band 3 binds to ankyrin, which in turn binds to β-spectrin in a specific region near the site of spectrin self-association. Ankyrin-band 3 junctions are not essential to the topological organization of the RBC membrane skeleton because lipid-extracted skeletons that have been stripped of accessory proteins and therefore do not contain these complexes retain the characteristic RBC skeletal geometry (Shen et al., 1986).

Conceptual models of the RBC membrane skeleton have been proposed by several investigators (Chasis and Mohandas, 1986; Shen, 1989; Ursitti and Wade, 1993; Nash and Gratzer, 1993; Mohandas and Evans, 1994). The consensus view is that the fundamental structural basis of RBC membrane elasticity is the reversible extension of spectrin molecules (Fig. 2). Spectrin is known to be an extensible molecule and has been visualized in configurations that span a range of lengths both in purified form and when bound to the RBC membrane skeleton (McGough and Josephs, 1990; Shen et al., 1986). In electron micrographs of

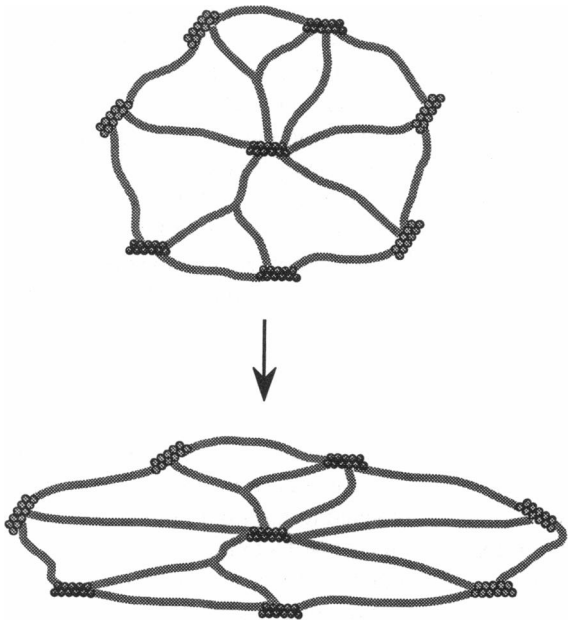

FIGURE 2 Conceptual model for deformation of the RBC membrane skeleton. Spectrin molecules become elongated in the direction of extension, but connections within the network are not altered.

asymmetrically stretched skeletons, the longest spectrin filaments tend to be aligned in the direction of extension (Liu et al., 1990; Liu et al., 1993). These observations support a model of skeletal deformation in which connections between spectrin molecules are relatively stable. Therefore, it is expected that the elasticity of the RBC membrane skeleton is primarily determined by the intrinsic elasticity of spectrin and the topology of the skeleton, meaning the organization of connections between spectrin molecules.

Previously, several quantitative models of the RBC membrane have been proposed that predict the contribution of the skeleton to gel-like elasticity (Stokke et al., 1986; Kozlov and Markin, 1987; Boal, 1994), diffusion of proteins within the membrane (Saxton, 1990), fracture behavior when spectrin links are broken (Grimson, 1993), relative motion of the skeleton and lipid bilayer during micropipette aspiration (Gaydos, 1994), and heterogeneity of skeletal density in axisymmetric deformations (Mohandas and Evans, 1994). Recently, Boal (1994) predicted several elastic parameters for the RBC membrane skeleton by assuming an entirely entropic origin for spectrin elasticity and constructing a network in which exactly six spectrin tetramers are joined at each actin junction. Each of these previous approaches toward modeling the contribution of skeletal structure to membrane mechanics applies to specific structural assumptions for skeletal topology and spectrin elasticity.

We have developed a computational model that is capable of incorporating a wide range of structural assumptions for the RBC membrane skeleton. One advantage of this model is the ability to include new information as more precise measurements become available for the topology of the native skeleton and the elasticity of spectrin. Secondly, significant variations in network topology (and possibly spectrin elasticity) are expected to be present among populations of normal and abnormal RBCs, thus affecting their mechanical behavior. By considering a range of structural assumptions, the model can be used to quantify the contributions of specific skeletal features to macroscopic mechanical properties. Here we discuss the implementation of the model for several choices of network topology and spectrin elasticity.

THE MODEL

The model presented here uses microstructural information about the RBC membrane skeleton as input, and the shear modulus (μ) and area expansion modulus (κ) of the skeleton are predicted as output. The model incorporates two essential features of the membrane skeleton: the topology of the skeleton and the elasticity of individual spectrin molecules. These features are represented mathematically in a two-dimensional finite element model in which spring-like elements correspond to spectrin, and nodes correspond to protein junctions in the RBC membrane skeleton. The model is versatile in the sense that a wide range of assumptions for network topology and spectrin elasticity may be considered, these two parameters may be varied independently of one another, and other structural features may be added, if needed.

After a network has been constructed with the desired topology and element elasticity, a representative sample region of the network is selected, and its mechanical properties are computed by finite element analysis. Deformations are imposed by prescribing the displacements for all nodes on the boundary of the sample region. The equilibrium configuration is computed for each deformed state, generating stresses and strains for each element, and the magnitude of any reaction forces that are present on the boundary nodes. Then the elastic moduli are computed for the corresponding effective continuum, using an appropriate constitutive law and the average response of the model network.

The computational procedures used in this model can be adapted for a wide variety of purposes. With minor modifications, this method may be used to simulate several types of mechanical phenomena, including elastic, viscoelastic, and plastic deformations of two-dimensional or three-dimensional materials. Several investigators have used similar methods to model the mechanical properties of other materials with random microstructures, including the fracture behavior of a two-dimensional lattice of springs (Beale and Srolovitz, 1988; Curtin and Scher, 1990), linear elasticity of planar random triangular networks (Ostoja-Starzewski and Wang, 1989, 1990), and the mechanics of granular (Satake, 1985) and fibrous materials (Arbabi and Sahimi, 1993). The present model is of the same type but is tailored to describe the RBC skeleton.

Representation of skeletal network topology

The topology of the RBC membrane skeleton can be characterized by the relative proportions of spectrin tetramers and hexamers, the average number of spectrin molecules per actin junction, and the distribution of dimer lengths. To develop a realistic model of skeletal topology, networks must be constructed by a method that makes it possible to control these features. A simple approach toward modeling the topology of the RBC membrane skeleton would be to extract all node and element positions directly from EM or AFM images of this structure. However, this method is limited by several factors, including the number of samples available, the size of the skeletal region visible in each image, and difficulties associated with identifying protein junctions in images of unstretched skeletons. Alternatively, a mathematical approach may be used to synthesize networks that replicate the known features of the skeleton. First, visualization data are used to obtain values for topological parameters such as the number of spectrin molecules per actin junction. Then, random networks with equivalent topologies are constructed mathematically. (Two networks with distinct node and element positions are considered to have equivalent topologies if they have the same topological parameters.) This method makes it possible to generate a number of networks of arbitrary size that are equivalent to a given topological configuration. Model networks may also be created for hypothetical topologies, for which images are not available, to study the sensitivity of μ and κ to parameter variations.

In this work, networks are synthesized by a Delaunay triangulation, as described in the Appendix. Nodes are assigned positions in a random fashion, and then edges are inserted systematically to create a network of triangles. Each edge in a Delaunay triangulation is considered to represent a spectrin tetramer, and each node corresponds to an actin junction. This type of network resembles a skeleton composed entirely of spectrin tetramers, with an average of six tetramers per actin junction. In the future, other topologies may be obtained by modifying the Delaunay triangulation. For example, spectrin hexamers may be added to this network by inserting Y-shaped sets of elements between the three vertices of any triangle. Using a combination of edge insertion and removal algorithms, the number of tetramers and hexamers as well as the average number of spectrin per actin junction may be adjusted. This approach makes it possible to construct networks that represent skeletons composed entirely of tetramers, entirely of hexamers, or any intermediate combination, and that span a range of spectrin densities as well. Furthermore, the average number of spectrin molecules per actin can be varied from as few as 3 to as many as 12.

Representation of spectrin elasticity

The contribution of spectrin elasticity to the deformability of the RBC membrane skeleton is included in the model by specifying the physical properties of elements of the network that coincide with the edges of a Delaunay triangulation. They may be modeled by elastic elements, such as linear or nonlinear central-force springs, or elastic beams. Nodes are assigned properties that are compatible with the selected element type. For example, central-force springs that do not resist bending but do exhibit a finite extensional stiffness must be joined together by freely rotating "pinned" joints. Elastic beams may be connected by either pinned or fixed joints.

Currently there is not enough information to quantify a precise stress-strain relationship for spectrin or to determine whether this protein provides significant resistance to bending or compression. The state of stress of spectrin in the native skeleton is also unknown. Observations of isolated skeletons suggest that spectrin may be unstressed (Svoboda et al., 1992) or may support a moderate degree of tension (Vertessy and Steck, 1989) in the native RBC membrane skeleton. As more information becomes available regarding the physical properties of a single spectrin molecule, it can be incorporated in this model. Furthermore, this model is not constrained to either an entropic or an energetic mechanism for spectrin elasticity, but it can incorporate both possibilities as well as intermediate conditions.

METHODS: IMPLEMENTATION OF THE MODEL FOR A PARTICULAR TYPE OF NETWORK

Here the elastic moduli are computed for a particular choice of network topology and spectrin elasticity. Specifically, it is assumed that all of the spectrin in the RBC membrane skeleton is present in tetrameric form and that an average of six tetramers are joined at each actin junction. Furthermore, it is assumed that the force-extension relationship for a single spectrin tetramer is linear and that spectrin tetramers form freely rotating connections at actin junctions. The mechanical properties of this network are computed and expressed in terms of a constitutive law for an equivalent two-dimensional isotropic finite elastic solid. Although this model network may not be an exact representation of the biological system, its simplicity makes it well suited for demonstrating our computational procedures in detail. In the future, the same methods will be used to study networks with more realistic models for skeletal topology and spectrin elasticity.

Creation of networks

The topology of a Delaunay triangulation is characterized by four parameters: the average junction functionality, $\bar{\phi}$; the standard deviation of junction functionality, σ_ϕ; the mean edge length, $\bar{L}$; and the standard deviation of edge length, σ_L. As a result of the inherent geometric properties of a planar Delaunay triangulation, the value of $\bar{\phi}$ is 6. Therefore, this type of network can be used to model the topology of the RBC membrane skeleton when it is assumed

that all spectrin is in tetrameric form, and an average of six tetramers are joined at each actin junction. For computational convenience, all networks are converted to a finite element representation with a common length scale of $\bar{L} = 1$. The remaining parameters, σ_ϕ and σ_L, are controlled by the network construction procedures, which are described in the Appendix. Sets of networks with equivalent topological statistics but different node and element positions are obtained by varying the seed value for the random number generator that is used to assign node positions.

Properties of the spectrin elements

The elasticity of spectrin is included in the model by assuming that each spectrin molecule behaves as a central-force spring with a linear force-extension relationship. In the RBC membrane skeleton, it is expected that each spectrin tetramer has the same rest length, L_o, and the same intrinsic elasticity, which we approximate with a spring constant, K. In general, spectrin elasticity may vary with extension. In a model network with random topology (i.e., $\sigma_\phi > 0$), the lengths of individual elements, L_i, will vary. Clearly, it is impossible to define a planar reference state for which all elements simultaneously satisfy $L_i = L_o$ and are therefore stress-free. Instead, a random network composed of identical springs (same L_o and K) is capable of supporting a residual stress field. Therefore, a rigorous analysis of this type of network would require the incorporation of residual stresses. To simplify the model and to make use of existing constitutive relations for the RBC membrane, we assume that all elements are unstressed in the reference configuration of the network.

The properties of the elements of a random network are defined herein in various ways. For each element i, we choose $K_i = K$, so that all elements have the same spring constant (type a). Alternatively, we define K_i as a function of the initial length of the element, L_i, so that $K_i = K\bar{L}/L_i$ (type b). Here, K is the mean value of the spring constant and corresponds to an edge with length $L_i = \bar{L}$, the mean edge length. Option b treats elements as if they have the same cross-sectional area, A, and are composed of material with the same Young's modulus, E, so that the quantity (EA/L_i) is the same for all elements in the network. When spring type a is used and truncated elements are generated by cutting out a region of the network, the spring constants of truncated elements are altered to reflect their length before truncation, rather than the length of the remaining portion. Then K is replaced by K/f_i, where f_i is the fraction of the length that is located inside the truncation boundary. Without this correction, truncated elements would be too compliant relative to the intact elements in the network. When spring type b is used, this correction is not needed.

In an equilateral triangular network, $L_i = \bar{L}$ for all elements, so spring types a and b are equivalent. We introduce "physical randomness" in such networks as follows: K_i is assigned randomly to produce a normal distribution of spring constants with mean value $\bar{K}$ and standard deviation σ_K.

Imposing a deformation on a sample region of the network

A finite sample region is selected to represent the structure and mechanical properties of a network that is assumed to extend indefinitely. To evaluate the importance of sample size and edge effects, each sample is subdivided into a "test region" and a "buffer region". The test region occupies a square at the center of the sample and contains N nodes as well as all elements that join two of these nodes. After a deformation, nodes and elements within the test region are used to compute the average principal extension ratios and the strain energy density for the network. The buffer region surrounds the test region and extends to the outer boundary of the network. This region acts as a buffer between the network boundary and the test region, in the sense that inhomogeneities introduced by applied forces or displacements at the outer boundary may become more dispersed before reaching the test region. Two different types of outer boundaries are considered: a "neighborhood boundary" and a "truncated boundary."

A neighborhood boundary is defined by a set of nodes for which the shortest path to the test region contains a particular number of elements characterized by the parameter B_n, a non-negative integer (Fig. 3, *a–c*). A "node" is a member of neighborhood boundary B_n if the shortest path between that node and the outer edge of the test region contains B_n elements. An "element" belongs to the B_n^{th} neighborhood if it joins a node of the B_n^{th} neighborhood boundary to another node on either the B_n^{th} or the $(B_n - 1)^{th}$ neighborhood boundary. When a network has no buffer region, its boundary is composed of the nodes on the outer edge of the test region, and this is called the $B_n = 0$ neighborhood boundary for the network. The model is used to test for the presence of edge effects by analyzing a series of samples in which the same test region is surrounded by buffer regions of different sizes.

A truncated outer boundary is defined by a square surrounding the test region that truncates elements it crosses (Fig. 3, *d–f*). Additional points are introduced as nodes of the network at each position where an element crosses the outer boundary. A truncated boundary is considered to be equivalent to a neighborhood boundary when the ratio of the number of nodes in the buffer region to the number of nodes in the test region, N_B/N, is the same in each network. The number of nodes in the buffer region, N_B, excludes nodes that are introduced by truncation. For a neighborhood boundary with some position B_n, the equivalent truncated boundary is characterized by the parameter B_t, with $B_t = B_n$.

A deformation of the model network is described in terms of the principal extension ratios of an equivalent two-dimensional continuum (Fig. 4). For a region with initial

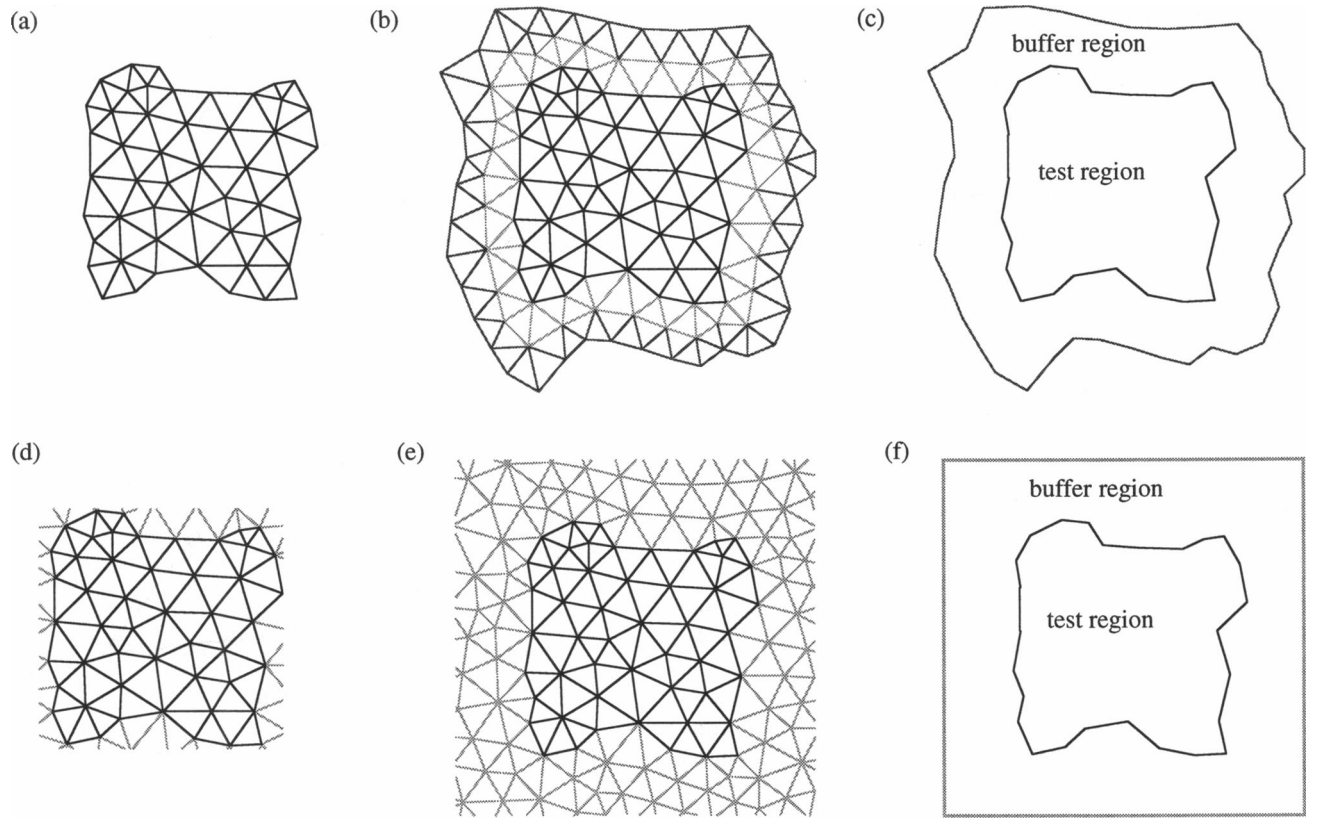

FIGURE 3 Defining a network sample region. (*a*) Neighborhood boundary position $B_n = 0$ contains only the test region. (*b*) Neighborhood boundary position $B_n = 2$ contains the test region as well as two surrounding "neighborhoods." (*c*) Illustration of the test region and buffer region when a neighborhood boundary is used. (*d*) Truncated boundary, with $B_t = 0$ (equivalent to $B_n = 0$). (*e*) Truncated boundary with $B_t = 2$. (*f*) Test region and buffer region in a truncated network.

dimensions dX_1 and dX_2 and deformed dimensions dx_1 and dx_2, the principal extension ratios are defined as $\lambda_1 = dx_1/dX_1$ and $\lambda_2 = dx_2/dX_2$. In a homogeneous deformation, λ_1 and λ_2 are constants throughout the part of the material considered. During isotropic expansion or compression, $\lambda_1 = \lambda_2$. When a region of the material undergoes pure shear at constant area, the extension ratios are related as $\lambda_1 = 1/\lambda_2$.

A particular deformation is imposed on the boundary nodes of the network by prescribing the displacements that they would undergo in a homogeneous deformation described by the principal extension ratios λ_1 and λ_2. For a point with initial coordinates (X_1, X_2), the displacement components are $u_1 = X_1(\lambda_1 - 1)$ and $u_2 = X_2(\lambda_2 - 1)$. After all constraints have been specified for the boundary nodes, the locations of all internal nodes are computed by the commercial finite element package ABAQUS (Hibbit, Karlsson, and Sorensen, RI). In ABAQUS, the coordinates of all nodes are specified for a desired length scale, and each element is defined in terms of the nodes at its endpoints. Springs are modeled by element type "SPRINGA." The deformed state of the network is computed using static analysis, with the "NLGEOM" option active to specify the

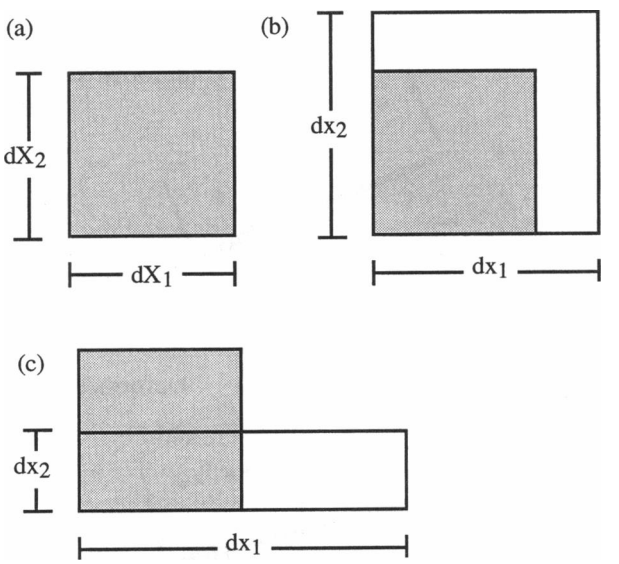

FIGURE 4 Description of a deformation in two dimensions. (*a*) Undeformed network; (*b*) isotropic expansion ($\lambda_1 = \lambda_2$); (*c*) pure shear at constant area ($\lambda_1 = 1/\lambda_2$).

use of nonlinear geometry. In computing the solution, internal nodes and elements are permitted to move freely within the plane to achieve equilibrium in the deformed state.

Computing an average description of network behavior

Principal extension ratios

Data from the finite element computations are used to compute the average strain field for nodes in the test region to verify that the network has experienced the expected average deformation. The deformed state of the network is characterized in terms of the components of Green's strain tensor, **E**. This Lagrangian measure of finite strain can be derived from the changes in the relative positions of a triad of points (see e.g., Waldman et al., 1985). Because the networks used in this analysis are composed of triangles, it is convenient to compute the strain for each individual triangle and to average the results over all triangles in the test region.

First, consider a single material line element (Fig. 5), with initial length Δs_o, where $(\Delta s_o)^2 = (\Delta X_1)^2 + (\Delta X_2)^2$. In the deformed configuration, this element has length Δs, where $(\Delta s)^2 = (\Delta x_1)^2 + (\Delta x_2)^2$. The change in length may be expressed as a function of the initial position and the strain components E_{11}, E_{12}, and E_{22}, assuming these are homogeneous within the triangle:

$$(\Delta s)^2 - (\Delta s_o)^2 = 2E_{ij}(\Delta X_i)(\Delta X_j) = 2E_{11}(\Delta X_1)^2 + 4E_{12}(\Delta X_1)(\Delta X_2) + 2E_{22}(\Delta X_2)^2 \quad (1)$$

To determine values for the three unknown strains E_{ij}, Eq. 1 must be applied to each of the three line elements of a triangle (Fig. 6). This yields a system of three linear equations in the form $[A]\{x\} = \{b\}$, where

$$[A] = \begin{bmatrix} 2(\Delta X_1^2)_p & 4(\Delta X_1 \Delta X_2)_p & 2(\Delta X_{2p}^2) \\ 2(\Delta X_1^2)_q & 4(\Delta X_1 \Delta X_2)_q & 2(\Delta X_2^2)_q \\ 2(\Delta X_1^2)_r & 4(\Delta X_1 \Delta X_2)_r & 2(\Delta X_2^2)_r \end{bmatrix},$$

and

$$\{b\} = \begin{bmatrix} (\Delta s^2 - \Delta s_o^2)_p \\ (\Delta s^2 - \Delta_o^2)_q \\ (\Delta s^2 - \Delta s_o^2)_r \end{bmatrix}, \quad (2)$$

in which the subscripts p, q, and r refer to the three sides of the triangle. The solution, $\{x\} = \{E_{11}, E_{12}, E_{22}\}$, is obtained by Gaussian elimination. The principal components E_1 and E_2 are the eigenvalues of **E**. The principal extension ratios λ_1 and λ_2 are related to E_1 and E_2 by:

$$\lambda_1 = (2E_1 + 1)^{1/2} \qquad \lambda_2 = (2E_2 + 1)^{1/2} \quad (3)$$

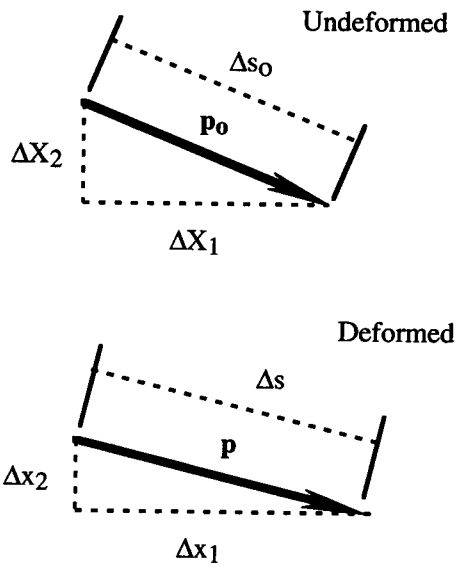

FIGURE 5 Single material line element undergoing a deformation.

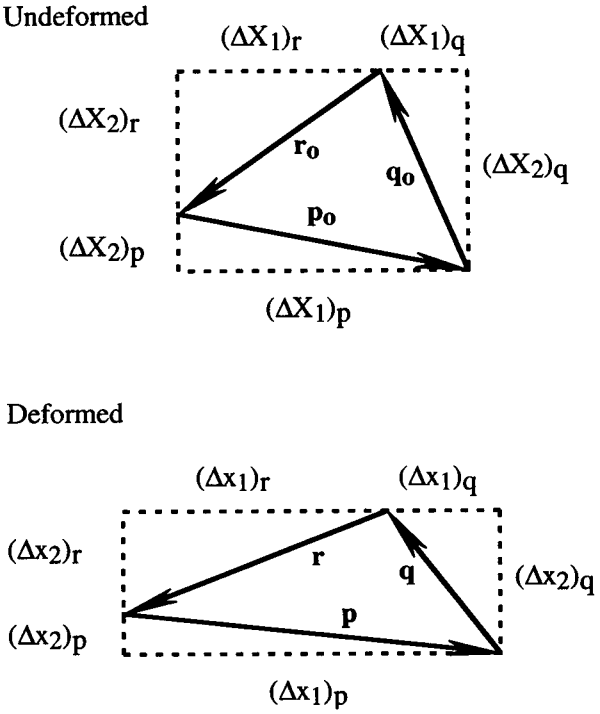

FIGURE 6 Computing finite strain from the deformation of a triad.

Principal components of Cauchy stress

The components of the Cauchy stress tensor, **T**, are computed from the reaction forces at the boundary nodes. Each boundary node is associated with reaction force components F_1 and F_2, relative to the x_1 and x_2 axes. Furthermore, a node is assigned to one of four sides of the network: left, right, top, and bottom, as indicated by the superscripts *l*, *r*, *t*, and *b*, respectively. The same notation is used to describe the reaction forces on either a truncated boundary (Fig. 7 *a*) or a neighborhood type of boundary (Fig. 7 *b*). In a truncated network, nodes are readily assigned to one of the four sides of the boundary. However, in a network with a neigh-

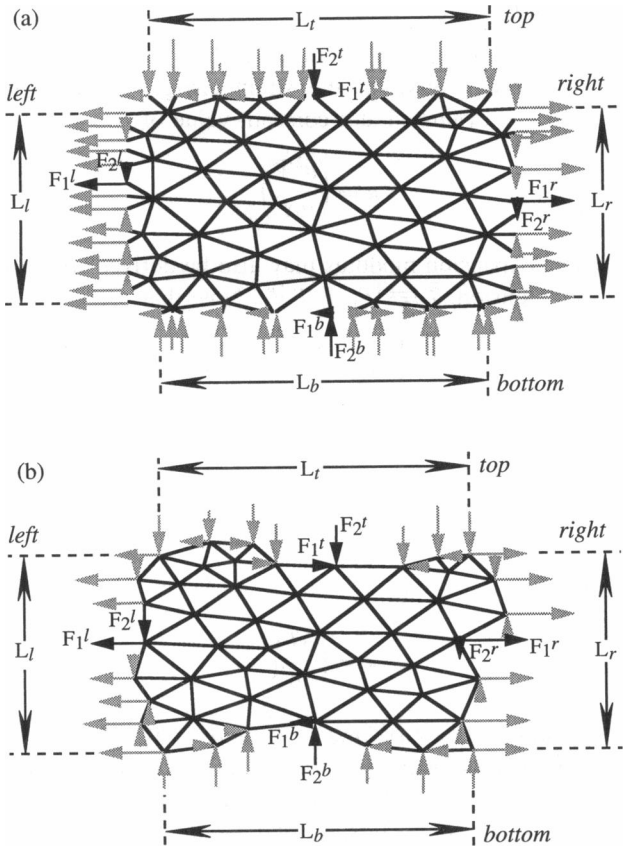

FIGURE 7 Identification of reaction force components. (*a*) Truncated boundary; (*b*) neighborhood boundary.

borhood boundary, this choice is more ambiguous because of the lack of distinct "corners." For purposes of this analysis, an ad hoc algorithm is applied. First, each node is given a set of ranks that describe its position along the x_1 and x_2 axes, relative to the other nodes. For example, the node with the highest valued x_1 coordinate would be ranked first among "right-most" nodes and ranked last among the "left-most" nodes. Similar lists are also generated for the top and bottom sides. A node is assigned to a particular side if it has the highest ranking on the list that corresponds to that side, relative to its ranks on the other three lists. The length of the right side, L_r is computed from the two nodes on that side with the maximum and minimum x_2 coordinates: $L_r = (x_2^r)_{\max} - (x_2^r)_{\min}$. Other side lengths are computed in a similar fashion. The length of each side is computed and denoted by L_l, L_r, L_t, and L_b. Any errors that result from this somewhat arbitrary procedure diminish as the number of nodes in the network increases.

In general, the nodal reaction forces on a particular side of the boundary are not identical. The equivalent Cauchy stresses are computed as the sum of the reaction forces on a side, divided by the length of that side in the deformed configuration. The average stresses on the two opposite sides of the network are used to compute each of the stress

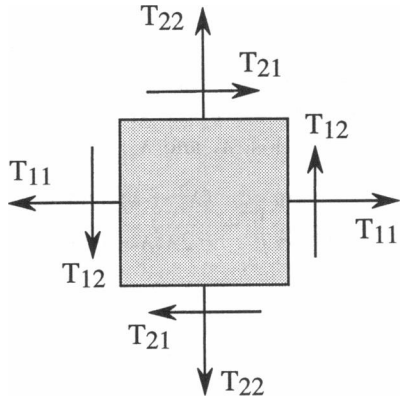

FIGURE 8 Components of the Cauchy stress tensor.

components (Fig. 8):

$$T_{11} = \frac{1}{2}\left(\frac{\sum F_1^r}{L_r} - \frac{\sum F_1^l}{L_l}\right) \qquad T_{12} = \frac{1}{2}\left(\frac{\sum F_2^r}{L_r} - \frac{\sum F_2^l}{L_l}\right) \tag{4}$$

$$T_{21} = \frac{1}{2}\left(\frac{\sum F_1^t}{L_t} - \frac{\sum F_1^b}{L_b}\right) \qquad T_{22} = \frac{1}{2}\left(\frac{\sum F_2^t}{L_t} - \frac{\sum F_2^b}{L_b}\right)$$

Although the Cauchy stress in a continuum is a symmetric tensor, and hence T_{12} and T_{21} are expected to be equal, these values are computed separately to evaluate the magnitude of any differences that may be present in this calculation. When the network is subjected to a homogeneous deformation that is aligned with the X_1 and X_2 axes, we expect $T_{12} = T_{21} = 0$, as in a continuum.

Strain energy density

Another measure of the average response of the network is the strain energy density in the test region. The strain energy density is computed as the sum, over all elements j in the test region, of the product of spring force, F_j, and extension relative to the initial spring length, ΔL_j:

$$\Psi = \frac{1}{2A_o}\sum_j F_j \Delta L_j \tag{5}$$

where A_o is the area of the test region in the reference configuration of the network. Elements that lie on the outer boundary of the network are assumed to contribute half of their strain energy to the sum in Eq. 5. Finally, we assume that the strain energy density of the network is equal to the strain energy of an associated effective continuum, under a homogeneous strain equal to the average strain of the network (Ostoja-Starzewski and Wang, 1990).

Elastic moduli computed from averaged data

The average response of the network is used to compute the elastic moduli for the corresponding effective continuum,

assuming a general two-dimensional constitutive law (Eq. 6) for an isotropic, homogeneous material undergoing finite elastic deformations (Evans and Skalak, 1980). The principal Cauchy stresses T_1 and T_2 are given as functions of the principal extension ratios, λ_1 and λ_2:

$$T_1 = \left[\left(\frac{\partial\Psi}{\partial\alpha}\right)_\beta + \frac{(\lambda_1^2 - \lambda_2^2)}{2\lambda_1^2\lambda_2^2}\left(\frac{\partial\Psi}{\partial\beta}\right)_\alpha\right],$$
$$T_2 = \left[\left(\frac{\partial\Psi}{\partial\alpha}\right)_\beta + \frac{(\lambda_2^2 - \lambda_1^2)}{2\lambda_1^2\lambda_2^2}\left(\frac{\partial\Psi}{\partial\beta}\right)_\alpha\right], \quad (6)$$

where Ψ is the strain energy density per unit of initial area. The two deformation parameters that are used in this formulation, α and β, are linearly independent functions of the principal extension ratios. α represents the fractional area expansion as $\alpha = \lambda_1\lambda_2 - 1$, and β describes the degree of pure shear in terms of the deformation of a circle into an ellipse: $\beta = ((\lambda_1^2+\lambda_2^2)/(2\lambda_1\lambda_2)) - 1$. The first term in the constitutive law corresponds to the stress due to area expansion, whereas the second represents the stress due to shear deformation. Although an applicable constitutive law may also be derived in terms of other measures of stress and strain, this particular formulation is chosen because it has been used previously to describe the behavior of the RBC membrane in micropipette aspiration experiments.

Shear modulus, μ

The shear modulus of the skeleton, μ, is defined as the derivative of the strain energy density, Ψ, with respect to β, for a constant value of α.

$$\mu \equiv \left(\frac{\partial\Psi}{\partial\beta}\right)_\alpha \quad (7)$$

Alternatively, the shear modulus may be obtained from the following expression for the maximum shear stress, $T_s \equiv |T_1 - T_2|/2$:

$$T_s = \frac{1}{2}|T_1 - T_2| = \frac{|\lambda_1^2 - \lambda_2^2|}{2\lambda_1^2\lambda_2^2}\left(\frac{\partial\Psi}{\partial\beta}\right)_\alpha; \quad (8)$$

so,

$$\mu = T_s/\lambda_s \quad (9)$$

where

$$\lambda_s = \frac{|\lambda_1^2 - \lambda_2^2|}{2\lambda_1^2\lambda_2^2}. \quad (10)$$

These two definitions for the shear modulus, Eqs. 7 and 9, are equivalent. In general, μ may be a function of the degree of deformation, $\mu = \mu(\alpha, \beta)$. For small strains and deformations in which area is constant, the above definitions of μ reduce to the usual ratio of shear stress to shear strain, $\mu = T_s/2e_s$, where $e_s = |\lambda_1^2 - \lambda_2^2|/4$.

Area expansion modulus, κ

The area expansion modulus of the skeleton, κ, is defined as the second derivative of the strain energy density with respect to α, evaluated at a constant value of β.

$$\kappa \equiv \left(\frac{\partial^2\Psi}{\partial\alpha^2}\right)_\beta \quad (11)$$

The area expansion modulus may also be derived from the isotropic tension, $\bar{T} \equiv |T_1 + T_2|/2$. Note that

$$\bar{T} = \frac{1}{2}(T_1 + T_2) = \left(\frac{\partial\Psi}{\partial\alpha}\right)_\beta, \quad (12)$$

so

$$\left(\frac{\partial\bar{T}}{\partial\alpha}\right)_\beta = \left(\frac{\partial^2\Psi}{\partial\alpha^2}\right)_\beta, \quad (13)$$

and hence

$$\kappa = \left(\frac{\partial\bar{T}}{\partial\alpha}\right)_\beta. \quad (14)$$

It is assumed that $(\partial\Psi/\partial\alpha) = 0$ at $\alpha = 0$. Then in the undeformed membrane ($\alpha = \beta = 0$), all stresses are zero, as was also assumed for the element definitions. Note that the two definitions for κ, Eqs. 11 and 14, are equivalent. For small strains, these definitions reduce to $\kappa = \bar{T}/\alpha$.

Poisson's ratio, ν

Poisson's ratio, ν, is another elastic parameter that is often used to characterize a two-dimensional isotropic membrane. Usually, ν is defined for small strains e_1 and e_2, in which case $\nu = -e_2/e_1$, where $T_1 > 0$ and $T_2 = 0$. For the case of large strains, ν may be defined in terms of the principal components of Green's strain, E_1 and E_2, when the membrane is subjected to uniaxial tension ($T_1 > 0$, $T_2 = 0$):

$$\nu = \frac{-E_2}{E_1} = \frac{-(\lambda_2^2 - 1)}{(\lambda_1^2 - 1)} \quad (15)$$

Poisson's ratio is related to the shear modulus and the area expansion modulus as follows (see e.g., Fischer, 1992):

$$\nu = \frac{\kappa - \mu}{\kappa + \mu} \quad \text{or} \quad \frac{\kappa}{\mu} = \frac{1 + \nu}{1 - \nu}. \quad (16)$$

We compute Poisson's ratio for the RBC membrane skeleton model as a means of testing the consistency of the computation of μ and κ in small deformations.

RESULTS

In evaluating the model results, several issues concerning the discrete nature of the networks arise. 1) The discrete nature of the model introduces mechanical variability among different networks with equivalent statistical topol-

ogies. Therefore, rather than drawing any conclusions from the response of a single network, it is advisable to compute mean values for elastic moduli, using sets of equivalent networks. 2) The predicted elastic moduli may be affected by the number of nodes and elements in a network. 3) The predicted elastic moduli may be affected by the shape and position of the network boundary. 4) The topology is only partially defined by the assumption that an average of six spectrin tetramers are joined at each actin junction ($\bar{\phi} = 6$). The standard deviation of junction functionality, σ_ϕ, and the standard deviation of edge length, σ_L, may also vary. 5) The shear modulus is not necessarily constant but may vary with the degree of deformation.

Elastic moduli have been computed for sets of networks with sizes ranging from $N = 50$ (50 nodes in the test region) to $N = 2000$. Unless otherwise specified, all networks have equivalent topologies characterized by $\bar{\phi} = 6.0$, $0.98 < \sigma_\phi < 1.07$, $\bar{L} = 1$, and $0.19 < \sigma_L < 0.25$. Each elastic element is assumed to be unstressed in the original configuration of the network and resists both tension and compression according to the linear spring type a, with $K_i = 1.0$, or type b, with $K_i = 1.0/L_i$, as defined previously.

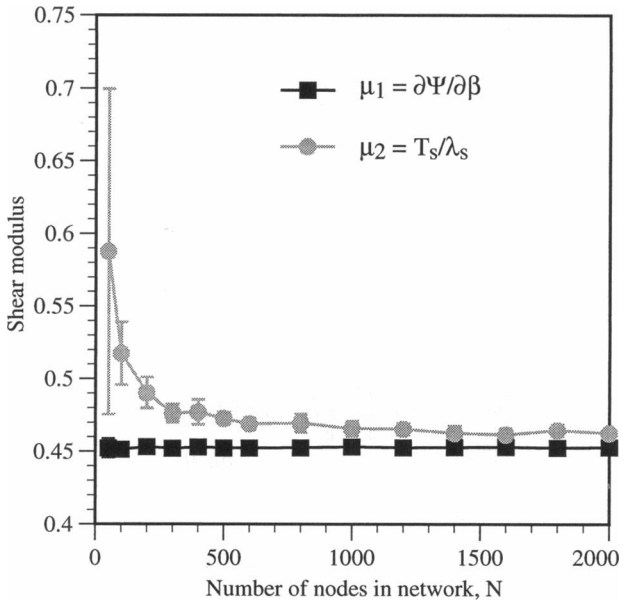

FIGURE 9 Shear modulus versus the size of the test region. Neighborhood boundary position $B_n = 0$. Error bars indicate standard deviation for 10 networks. $K = 1.0$ for all elements.

Computation of μ

We begin by computing the shear modulus, μ, at $\alpha = 0$ and $\beta = 0$, so that the results may be compared with μ as predicted by small deformation theory. As discussed in the previous section, the shear modulus may be derived from two equivalent formulas, which we denote by μ_1 and μ_2:

$$\mu_1 = \left(\frac{\partial \Psi}{\partial \beta}\right) \quad \text{and} \quad \mu_2 = \left(\frac{T_s}{\lambda_s}\right) \tag{17}$$

The values of Ψ, β, and λ_s are based on the behavior of the test region, whereas T_s depends on the reaction forces on the outer boundary of the network. Because μ_1 and μ_2 are derived from averages over different parts of the network, we expect to demonstrate equivalence of μ_1 and μ_2 only when the test region is sufficiently large and the boundaries are well defined.

The predicted value of the shear modulus varies with N, the number of nodes in the test region, as shown in Fig. 9. The computed shear modulus decreases as N is increased, as is expected when continuum constitutive coefficients are derived from a discrete material model using a uniform strain approximation (Ostoja-Starzewski and Wang, 1990). The effective shear modulus approaches a steady value as the size of the sample region becomes large relative to the size of the discrete features within the material. Of the two definitions considered, the computed value of μ_2 is more sensitive to such finite size effects. The amount of scatter exhibited among equivalent networks also decreases as N increases.

The shear modulus also varies with the type of boundary that surrounds the sample network. Recall that the position of a neighborhood boundary is given by B_n, and the position of a truncated boundary is denoted by B_t. In either type of network, the total number of nodes is N_T. The effect of the neighborhood boundary position B_n on the predicted value of the shear modulus is shown for both μ_1 and μ_2 (Fig. 10, *a* and *b*) as functions of N_T. Regardless of the size of the test region, the shear modulus is more strongly affected by N_T than by B_n, particularly when the definition for μ_2 is used. For example, similar results are obtained for networks with $N = 100$, $B_n = 2$ (average $N_T \approx 194$) and $N = 200$, $B_n = 0$ ($N_T = 200$). In Fig. 11, plots of μ_1 and μ_2 are superimposed for a few values of N, indicating that the agreement between μ_1 and μ_2 improves as N_T increases. Similar effects are observed when the position of a truncated boundary is increased, as shown in Fig. 12.

Computation of κ

The area expansion modulus may also be computed by two equivalent formulas, which we denote by κ_1 and κ_2:

$$\kappa_1 = \left(\frac{\partial^2 \Psi}{\partial \alpha^2}\right) \quad \text{and} \quad \kappa_2 = \left(\frac{d\bar{T}}{d\alpha}\right) \tag{18}$$

As was the case for the shear modulus, the predicted values of κ_1 and κ_2 decrease as N is increased (Fig. 13). The difference between κ_1 and κ_2 is smaller when the test region is larger, regardless of the type of boundary definition that is used.

Computation of ν

Poisson's ratio is computed by three methods. Two values are obtained from the shear modulus and area expansion

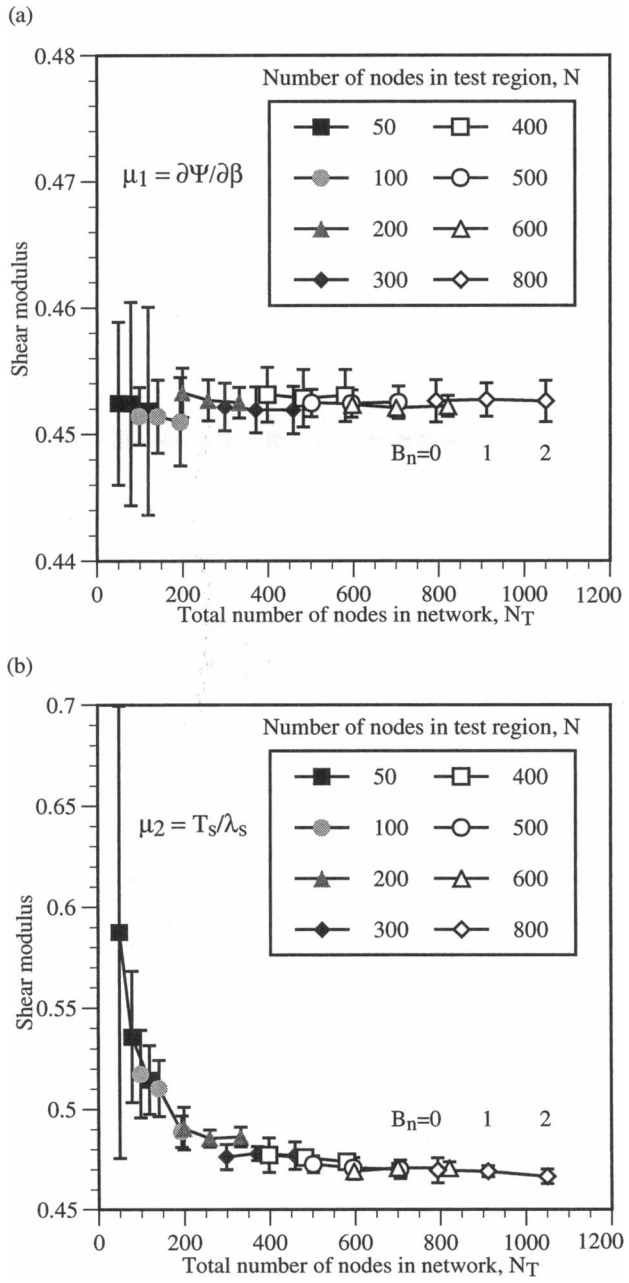

FIGURE 10 (a) μ_1 versus the total number of nodes in the network, N_T; (b) μ_2 versus N_T. Neighborhood boundary positions B_n = 0, 1, and 2 are indicated for networks with N = 800. Error bars indicate standard deviation for 10 networks. K = 1.0 for all elements.

modulus as $\nu_1 = (\kappa_1 - \mu_1)/(\kappa_1 + \mu_1)$ and $\nu_2 = (\kappa_2 - \mu_2)/(\kappa_2 + \mu_2)$. Then a third value, denoted by ν_3, is computed by using Eq. 15. Networks are subjected to a series of small deformation steps where λ_1 is held constant and λ_2 is varied. Then, assuming that T_2 varies linearly with λ_2, it is determined which value of λ_2 corresponds to $T_2 = 0$. The resulting values for ν_1, ν_2, and ν_3 are given in Fig. 14. All three methods for computing Poisson's ratio exhibit dependence on N, with a considerable amount of scatter. Among these values, ν_1 is likely to provide the most reliable esti-

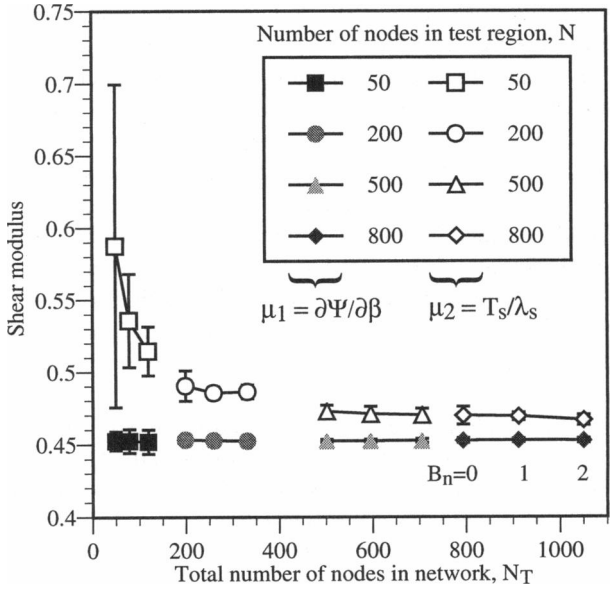

FIGURE 11 Comparison of μ_1 and μ_2 versus N_T for selected values of N. Neighborhood boundary positions B_n = 0, 1, and 2 are indicated for networks with N = 800. Error bars indicate standard deviation for 10 networks. K = 1.0 for all elements.

mate because ν_2 and ν_3 are both subject to errors due to boundary irregularities. For large N, $\nu_1 \approx \frac{1}{3}$, which corresponds to a ratio of $\kappa/\mu = 2$. This result computed for random networks is consistent with the value of $\nu = \frac{1}{3}$ that is expected for an equilateral triangular network composed of linear springs.

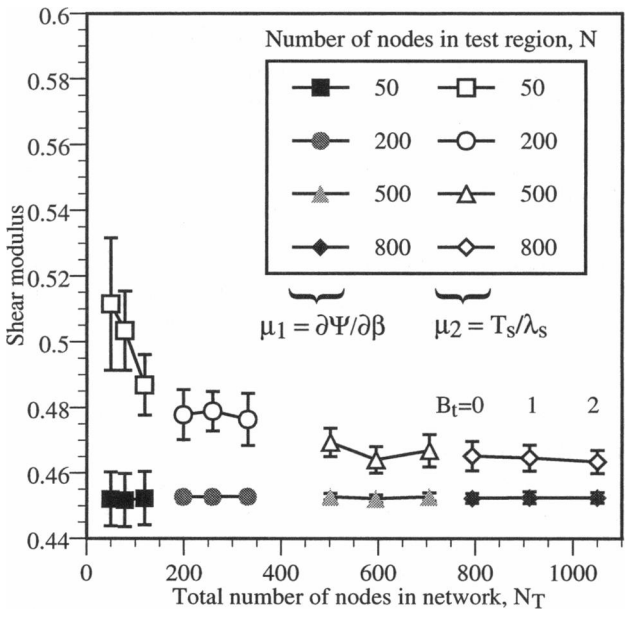

FIGURE 12 Comparison of μ_1 and μ_2 versus N_T for selected values of N. Truncated boundary positions B_t = 0, 1, and 2 are indicated for networks with N = 800. Error bars indicate standard deviation for 10 networks. K = 1.0 for all elements.

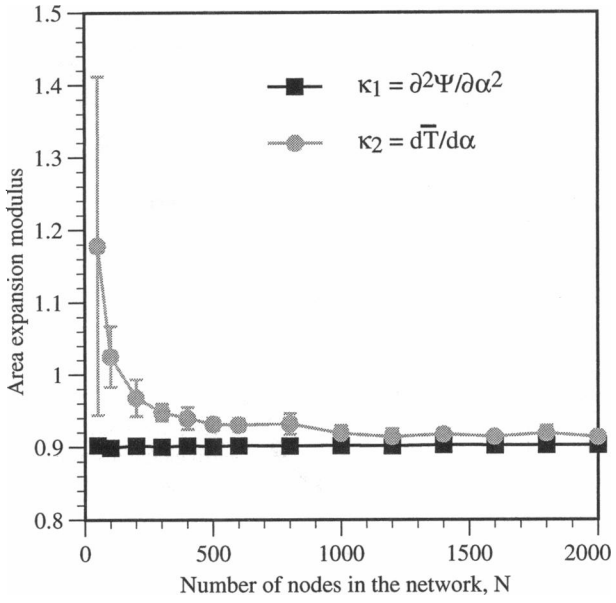

FIGURE 13 Area expansion modulus versus the size of the test region. Neighborhood boundary position $B_n = 0$. Error bars indicate standard deviation for 10 networks. $K = 1.0$ for all elements.

Effect of network randomness on the predicted values of μ and κ

Triangular networks may be constructed with a particular degree of "spatial randomness," as characterized by the standard deviation of edge length, σ_L, and the standard deviation of the number of edges per node, σ_ϕ. In this context, σ_L is normalized relative to a mean edge length of $\bar{L} = 1$.

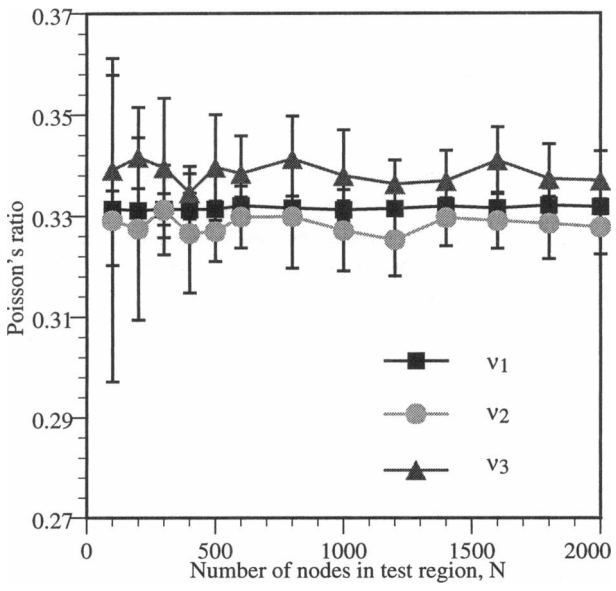

FIGURE 14 Poisson's ratio versus the size of the test region: $\nu_1 = (\kappa_1 - \mu_1)/(\kappa_1 + \mu_1)$; $\nu_2 = (\kappa_2 - \mu_2)/(\kappa_2 + \mu_2)$; $\nu_3 = -E_2/E_1$ ($T_1 > 0$, $T_2 = 0$). Neighborhood boundary position $B_n = 0$. Error bars indicate standard deviation for 10 networks. $K = 1.0$ for all elements.

The elastic moduli of an equilateral triangular network composed of linear central-force springs may be predicted by mean field theory (see e.g., Boal et al., 1993). For small deformations, the change in energy per unit cell (1 node + ½ of each adjoining element) is computed for pure shear and for isotropic area change, yielding predictions of $\mu = (\sqrt{3})/4 = 0.433$ and $\kappa = (\sqrt{3})/2 = 0.866$ and consequently $\nu = ⅓$. When the computational procedures for our RBC membrane skeleton model are applied to equilateral triangular networks, we obtain the mean field values for μ and κ.

Random networks were constructed to span a range of values for σ_L and σ_ϕ. Both σ_L and σ_ϕ affect network elasticity, and different combinations of these values may result in either an increase or a decrease in elastic moduli. It was reported previously that network stiffness is reduced as the degree of spatial randomness is increased (Ostoja-Starzewski and Wang, 1989). These results are replicated with our model when the randomness is introduced by two methods: 1) introduction of disorder to an equilateral triangular network and 2) specification of a minimum distance that is maintained between any two nodes in the network (see Appendix). Over a range of $\sigma_L = 0$ to 0.5 (Fig. 15 *a*), and $\sigma_\phi = 0$ to 1.4 (Fig. 15 *b*), the shear modulus decreases by as much as 50%, and the area expansion modulus decreases by up to 60% (data not shown). However, when the topology is modified through the use of a mechanical relaxation procedure in which all springs are treated as if they have a rest length of zero (see Appendix), then the stiffness of the networks is increased in the more random networks by up to 10%. This apparent contradiction is clarified by considering the relationship between σ_L and σ_ϕ (Fig. 16 *a*). When randomness is controlled by introducing disorder in an equilateral triangular network, σ_L and σ_ϕ exhibit a nearly linear relationship. If these networks are then subjected to mechanical relaxation, σ_L for a particular network will be reduced but σ_ϕ will not change. Pairs of values for σ_L and σ_ϕ that lie in the upper left region of the contour plot (Fig. 16 *b*) are associated with an increase in network stiffness. One possible explanation for this phenomenon is that networks with relatively large values for σ_ϕ tend to contain more nodes that are connected to only three or four edges. When the randomness of ϕ and L are independently assigned, there is no correlation between the length of an edge and the functionality of the nodes to which it is connected (Fig. 17, *a* and *b*). However, when network randomness is modified by mechanical relaxation, a correlation may arise between ϕ and the lengths of adjacent elements (Fig. 17, *c* and *d*). Neighboring edges tend to be shorter than average when ϕ is less than 6, and longer than average when ϕ is greater than 6. It is found that networks with such clustering behavior can exhibit an increase in stiffness relative to purely random networks.

Another effect of network randomness on elasticity is illustrated by assigning random spring constants to the elements of a regular network. The mean spring constant is

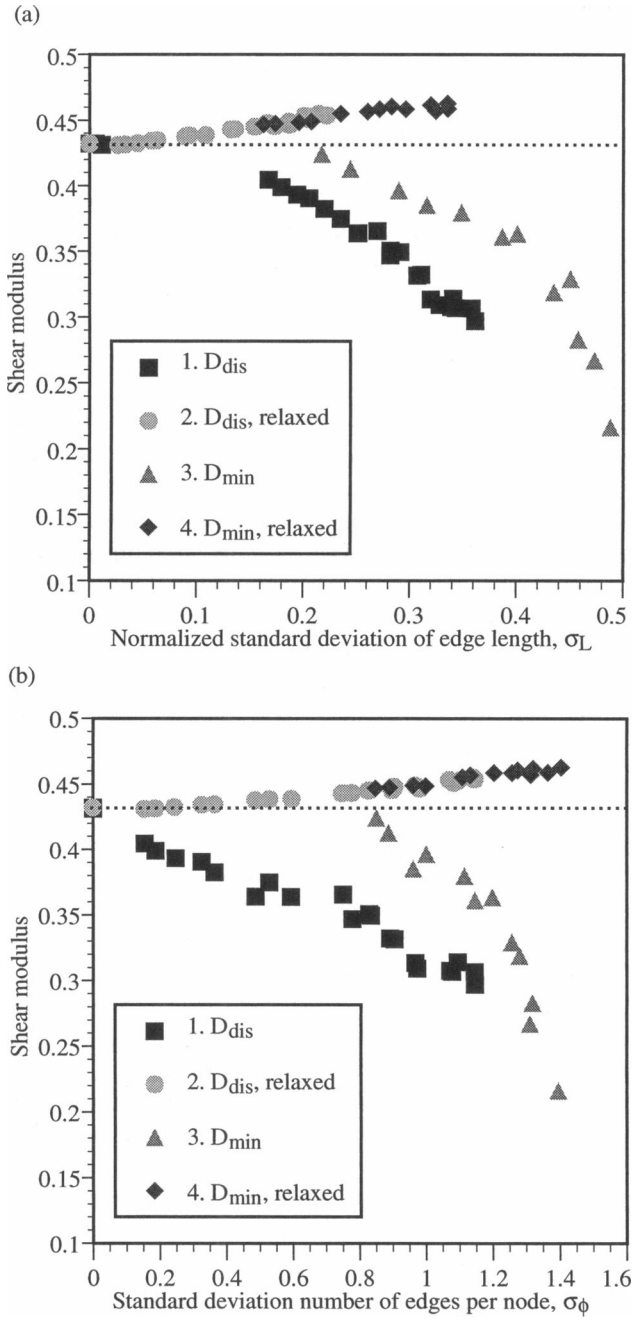

FIGURE 15 Shear modulus as a function of network randomness. (*a*) $\mu = \partial\Psi/\partial\beta$ versus the normalized standard deviation of edge length, σ_L. (*b*) $\mu = \partial\Psi/\partial\beta$ versus the standard deviation of the number of edges per node, σ_ϕ. Four methods for controlling network randomness are compared: 1) D_{dis}, disorder is introduced to each node of a regular network; 2) D_{dis}, relaxed, same procedure as 1, followed by mechanical relaxation of the network; 3) D_{min}, minimum distance constraint; 4) D_{min}, relaxed, same as 3, followed by mechanical relaxation of the network. Dashed lines indicate the value of $\mu = 0.433$, which is obtained from mean-field approximations when $K = 1.0$. $N = 1000$, $B_n = 0$, $K = 1.0$.

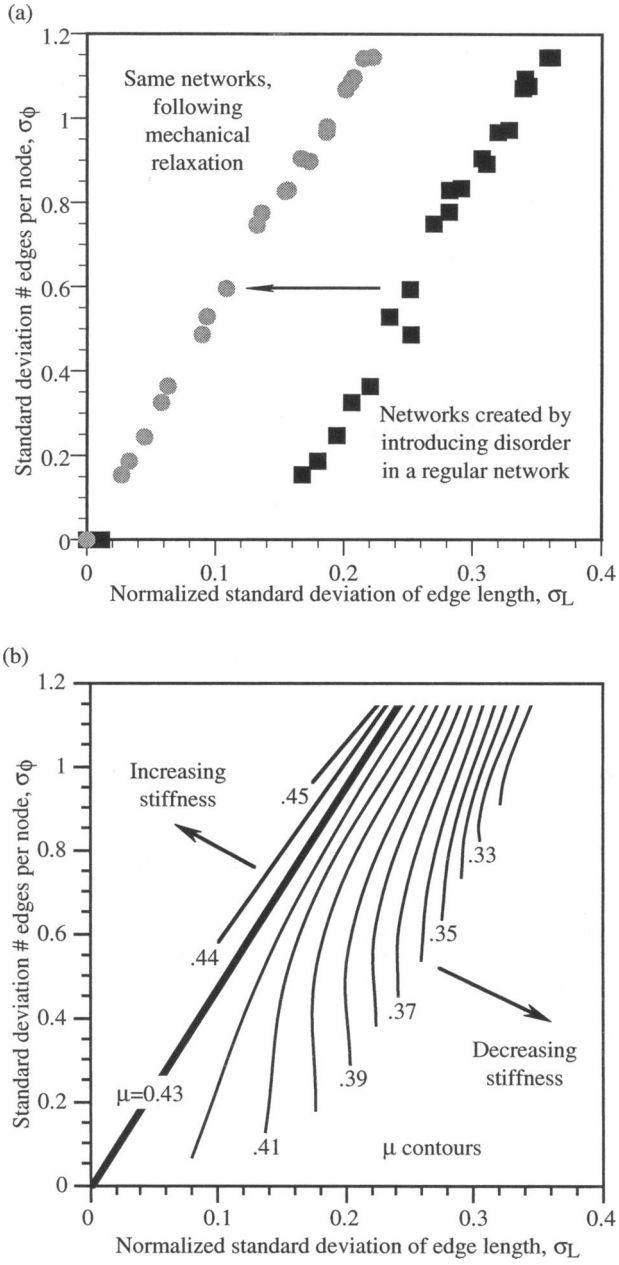

FIGURE 16 (*a*) Range of values obtained for the normalized standard deviation of edge length, σ_L, and the standard deviation of the number of edges per node, σ_ϕ, by introducing disorder in an equilateral triangular network. σ_L is decreased in the "relaxed" networks, but σ_ϕ is not changed. (*b*) Shear modulus as a function of network randomness. Contour plot of $\mu = \partial\Psi/\partial\beta$ versus σ_L and σ_ϕ. $N = 1000$, $B_n = 0$, $K = 1.0$. The contours shown are approximate and are obtained by smoothing plots from one case of each pair of σ_L and σ_ϕ tested.

held at $K = 1.0$, and the standard deviation σ_K is varied. As shown in Fig. 18, the resulting decrease in shear modulus is similar to the effects of varying σ_L by the specification of a minimum distance constraint D_{min} or by the introduction of some degree of disorder, D_{dis}, in an equilateral triangular network.

Effect of stretch λ_1 on μ

In the previous sections, all elastic moduli are computed for small deformations and are therefore comparable to the

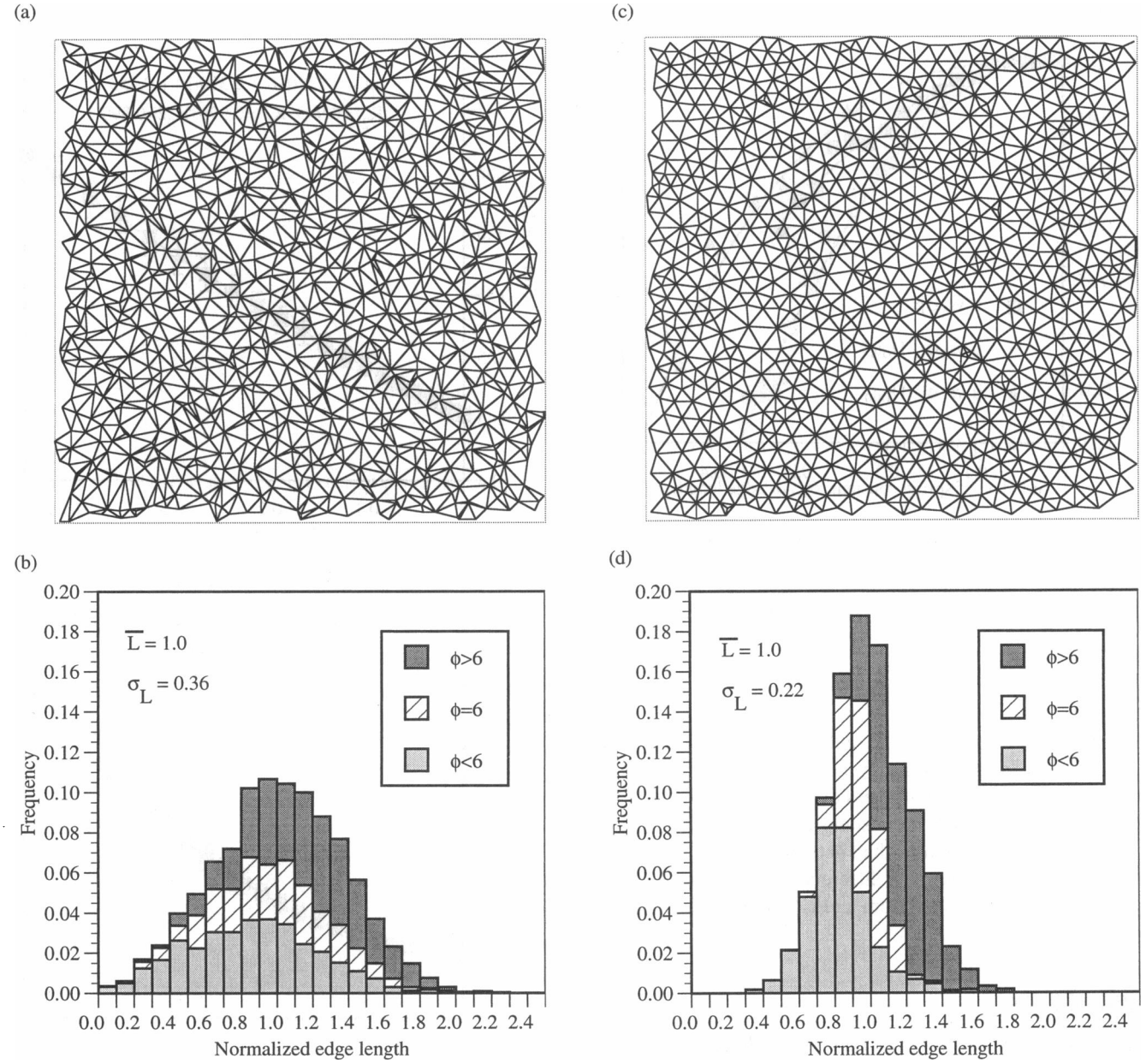

FIGURE 17 (*a*) Network created by introducing disorder in an equilateral triangular network, $D_{dis} = 0.80$, $N = 1000$. (*b*) Distribution of edge lengths as a function of average junction functionality of an edge: $\phi = (\phi_1 + \phi_2)/2$, where ϕ_1 and ϕ_2 are the number of edges joined to each of the endpoints of an edge. (*c*) Same network as shown in (*a*), following mechanical relaxation. (*d*) Distribution of edge lengths as a function of ϕ in the relaxed network.

results that have been predicted by models based on linear elastic constitutive formulations. However, the RBC membrane skeleton undergoes large extensional deformations in vivo, and many techniques that are used to measure the elastic shear modulus also induce large deformations. Our modeling procedure, which is applicable to large deformations, is used to compute the shear modulus as a function of extension (Fig. 19). As λ_1 increases from 1.0 to 1.5, with $\lambda_2 = 1/\lambda_1$ to preserve the total area of the network, μ increases from 0.45 to 0.62 (+35%). The shear modulus varies as a quadratic function of β or as a third-order polynomial function of λ_1.

Effect of the spring constant definition on μ and κ

The results shown in Figs. 10–17 and Fig. 19 are computed for networks composed of springs that have the same spring constant $K = 1$ (type a). When the spring constants are assigned according to spring definition type b, where $K_i = 1/L_i$, most qualitative aspects of network behavior are not altered. For example, the agreement between μ_1 and μ_2, as well as κ_1 and κ_2, improves as N increases for any choice of neighborhood boundary position B_n or truncated boundary position B_t. The dependence of the shear modulus on ex-

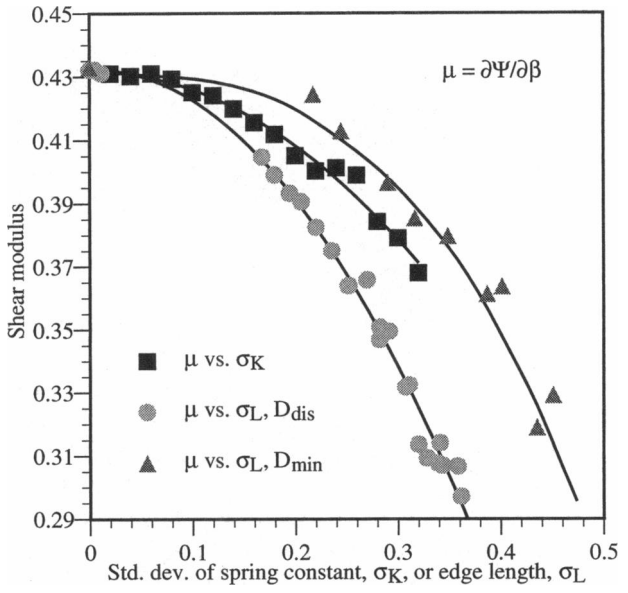

FIGURE 18 Shear modulus as a function of the standard deviation of spring constant, σ_K, for an equilateral triangular network with random spring constants, as compared with μ as a function of the standard deviation of edge length, σ_L, for networks with randomness controlled by varying D_{dis} or D_{min}. $N = 1000$, $B_n = 0$.

tension is also the same for either spring type a or b. However, the spring constant definition does affect the influence of network randomness on network elasticity (Fig. 20). Networks with spring constants assigned as $K_i = 1.0/L_i$ (type b) are generally stiffer than networks in which $K = 1.0$ for all elements (type a). The difference in μ increases as the networks become more random and is as large as 20% when $\sigma_L = 0.35$.

DISCUSSION

The model of the RBC membrane skeleton developed herein is capable of incorporating a variety of assumptions for both skeletal topology and spectrin elasticity. The computations demonstrate the implementation of the model for one particular choice of skeletal topology and spectrin elasticity. The same methods may be used to compute the elastic moduli for model networks that are based on other assumptions for RBC skeletal structure, such as incorporating elements that posses bending stiffness.

The discrete nature of this model introduces an influence of finite size effects on the predicted values of μ and κ. For a triangular network with a particular degree of randomness, the predicted values of μ and κ decrease as the number of nodes in the network is increased. Among networks with equivalent topological statistics, the scatter in elastic moduli also decreases as the number of nodes increases. The most consistent values are computed with the strain energy-based definitions μ_1 and κ_1 for networks containing at least 500 nodes. For example,

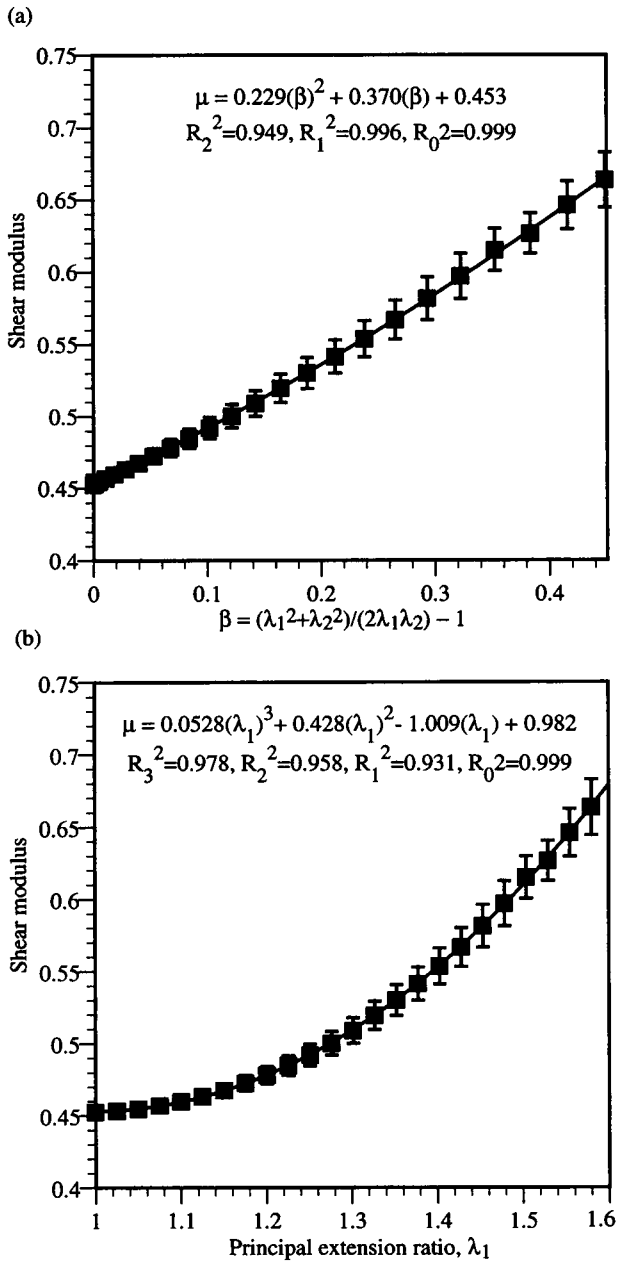

FIGURE 19 Shear modulus as a function of extension. (*a*) μ versus β, (*b*) μ versus λ_1. Error bars indicate standard deviation for 10 networks, $N = 500$, $B_n = 0$, $K = 1.0$.

μ_1 varies by only 0.1% among networks with 500-2000 nodes in the test region. For this range of N, the predictions of the model are not affected significantly by the choice of a truncated or neighborhood type of boundary. For a particular test region, a network with a truncated boundary ($B_t = 0$) contains many more nodes than a network with a neighborhood boundary ($B_n = 0$). Therefore we use networks with neighborhood boundary position $B_n = 0$ to minimize processing time.

Most of the values for μ and κ reported in this paper correspond to networks in which the linear spring constant

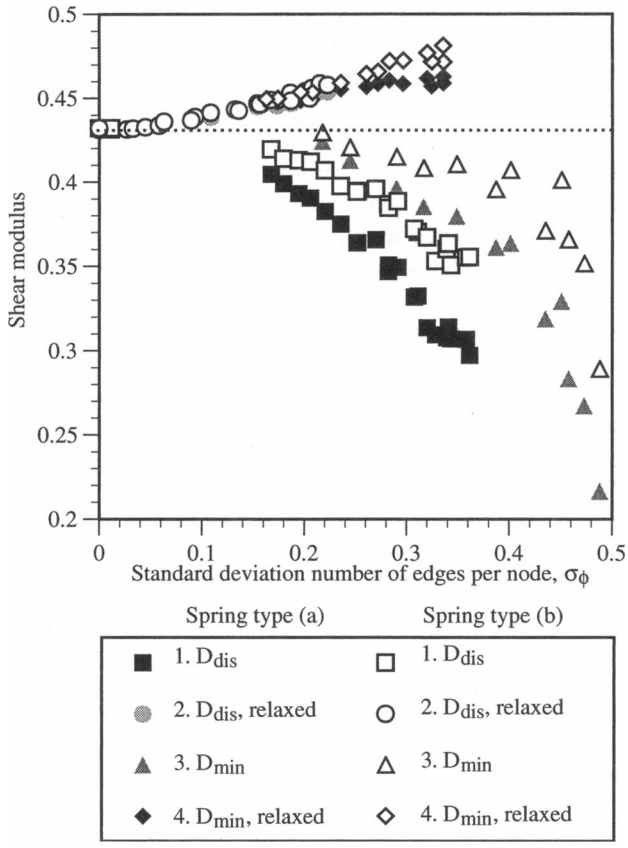

FIGURE 20 Shear modulus as a function of network randomness. For spring type a, $K = 1.0$ for all elements, and for spring type b, $K = 1.0/L_i$ for all elements, where L_i is the length of a particular element in the undeformed configuration of the network. Four methods for controlling network randomness are compared: 1) D_{dis}, disorder is introduced to each node of a regular network; 2) D_{dis}, relaxed, same procedure as 1, followed by mechanical relaxation of the network; 3) D_{min}, minimum distance constraint; 4) D_{min}, relaxed, same as 3, followed by mechanical relaxation of the network. The dashed line indicates the value of $\mu = 0.433$, which is obtained from mean-field approximations when $K = 1.0$. $N = 1000$, $B_n = 0$.

K is equal to 1.0 for all elements (type a). For networks with the same topology, other values for μ and κ are obtained by specifying some other value for K and maintaining the same dimensionless ratios μ/K and κ/K. Conversely, given a measured value for μ or κ, we can compute the corresponding value for the spring constant K using these dimensionless ratios.

The micropipette aspiration technique commonly used to measure the shear modulus of the intact RBC membrane yields a value of $\mu_m = 6\text{–}9 \times 10^{-3}$ dyn/cm (Chien et al., 1978; Waugh and Evans, 1979; Hochmuth, 1987). If we assume that the shear modulus of the membrane is the same as the shear modulus of the isolated skeleton, $\mu_m \approx \mu$, then the computed ratio of $\mu/K = 0.45$ predicts $K = 1.3\text{–}2.0 \times 10^{-2}$ dyn/cm for spectrin as a linear spring.

In actuality, the skeleton does not deform homogeneously when the RBC membrane undergoes micropipette aspiration, as has been demonstrated by fluorescence microscopy of antibody-labeled protein components (Discher et al., 1994). Although the overall membrane area remains constant, the skeleton moves relative to the lipid bilayer and undergoes local area dilation and compression. Therefore, rather than equating the shear modulus of the membrane to the shear modulus of the skeleton as $\mu_m \approx \mu$, we expect contributions from both μ and κ of the skeleton. Mohandas and Evans (1994) have proposed a serial coupling of these parameters, as $\mu_m \approx (\mu\kappa)/(\mu + \kappa)$. This formula yields an increase in the predicted value of K for a spectrin element, as shown in Table 1.

In previous computational models of the RBC membrane skeleton based on mean-field approximations (Stokke et al., 1986; Kozlov and Markin, 1987) and small deformation theory (Boal, 1994), μ is implicitly defined as a constant parameter. Our model, which is applicable to large deformations, predicts that μ increases as a cubic function of λ_1, where $\lambda_2 = 1/\lambda_1$ (Fig. 19). This behavior is reasonable because the spring elements in the model network are permitted to rotate and become aligned with the direction of extension. Experimental measurements of the RBC membrane are typically used to compute a constant value for μ_m. However, these data do not exclude the possibility that μ_m varies with λ_1; in most cases, the uncertainty in μ_m is greater than the 30% change in μ that we predict with our model. If we assume that the measured value of μ_m applies to a deformation at constant area and with an extension ratio of $\lambda_1 = 1.5$ and use our computed value of $\mu = 0.62$, then smaller values for K are predicted (Table 1). This is probably a more realistic value because local deformations in the pipette are quite large.

The area expansion modulus of the isolated skeleton, κ, has not been measured because it is several orders of magnitude smaller than the area expansion modulus of the lipid bilayer component of the membrane, κ_m. However, a ratio of $\kappa/\mu \approx 2.0$ has been estimated by comparing continuum models with the observed distribution of skeletal density along the length of the aspirated portion of the RBC membrane in micropipette experiments (Mohandas and Evans, 1994). A similar result is obtained by Boal (1994): $\kappa/\mu = 1.7$. For an equilateral triangular network composed of linear central-force springs, mean field approximations yield a value of $\kappa/\mu = 2.0$. These results from diverse approaches are in the same range as predictions of the

TABLE 1 Predicted values for spectrin elasticity in terms of a linear spring constant, K, computed for extension ratios $\lambda_1 = 1.0$ and 1.5, and two different assumptions for the measured red blood cell membrane shear modulus, μ_m

λ_1	Computed value for μ/K	Computed value for κ/K	Assumed relation of μ_m to μ and κ	Range of values for K, dyn/cm
1.0	0.45	0.90	$\mu_m \approx \mu$	$1.3 - 2.0 \times 10^{-2}$
1.0	0.45	0.90	$\mu_m \approx \mu\kappa/(\mu + \kappa)$	$2.0 - 3.0 \times 10^{-2}$
1.5	0.62	0.90	$\mu_m \approx \mu$	$0.97 - 1.5 \times 10^{-2}$
1.5	0.62	0.90	$\mu_m \approx \mu\kappa/(\mu + \kappa)$	$1.6 - 2.5 \times 10^{-2}$

models presented herein ($\kappa/\mu = 2$ for $\lambda_1 = 1.0$, $\kappa/\mu = 1.5$ for $\lambda_1 = 1.5$). Although some changes in κ/μ may result from changes in topology or from large deformations, the general agreement of predictions of the model with the experimental data suggests that the essential physical properties of the RBC membrane skeleton are well represented by a network of springs.

As shown in Figs. 15, 16, and 20, changes in the randomness of the topology of a model network may alter the predicted value of the shear modulus by 20% or more. Currently, the degree of randomness in the native RBC membrane skeleton is unknown. For purposes of testing the effects of network size (N) and boundary type (B_n and B_t) on the predicted values of μ and κ, we chose to use networks with a moderate degree of randomness characterized by $\sigma_L = 0.22$ and $\sigma_\phi = 1.05$. Similar results are obtained for other degrees of network randomness, although the degree of scatter among topologically equivalent networks generally increases as the network randomness increases. More importantly, these results serve as a means of demonstrating that elastic moduli are affected by network randomness. Models based on equilateral triangular networks will not necessarily yield the same predictions as models that make use of random topologies. As more accurate statistical data for RBC skeletal topology are established and are incorporated in the model (e.g., changing the fractions of spectrin tetramers and hexamers), it is anticipated that the effects of topological variations on the shear modulus will be even more pronounced.

In the future, we also intend to model abnormal RBC membrane skeletons and compare the predicted elastic moduli with the measured properties of abnormal RBC membranes. Various structural modifications of the skeleton have been associated with significant changes in the membrane shear modulus μ_m. For example, μ_m is reduced in cells with spectrin-deficient skeletons, suggesting that the density of spectrin is an important structural feature of the skeleton (Waugh and Agre, 1988). The connectivity of spectrin molecules within the skeleton also affects membrane deformability in shear, as evidenced by the change in μ_m observed for membranes with impaired self-association (Chabanel et al., 1989). Analysis of abnormal RBCs may provide clues regarding likely functional roles for specific structural features of the skeleton.

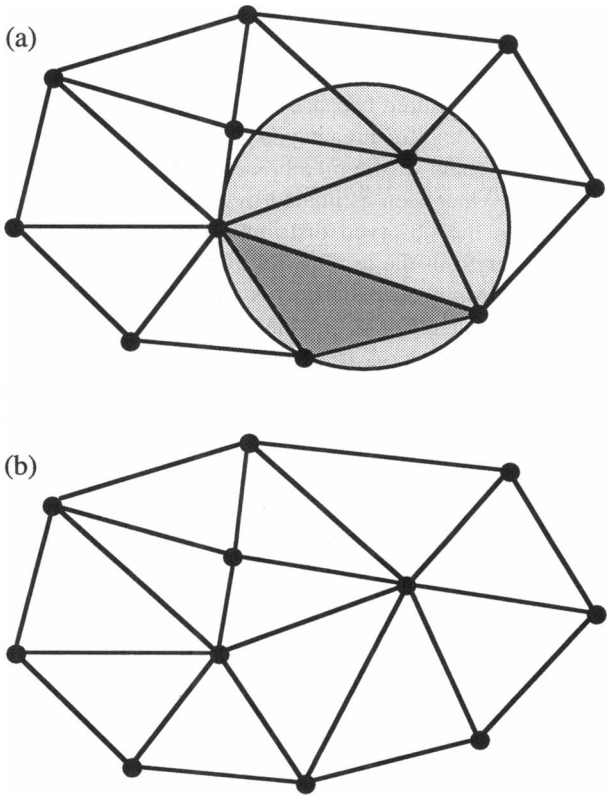

FIGURE A1 (*a*) A nonempty circumcircle in an arbitrary triangulation; (*b*) a Delaunay triangulation obtained by swapping one edge in the arbitrary triangulation.

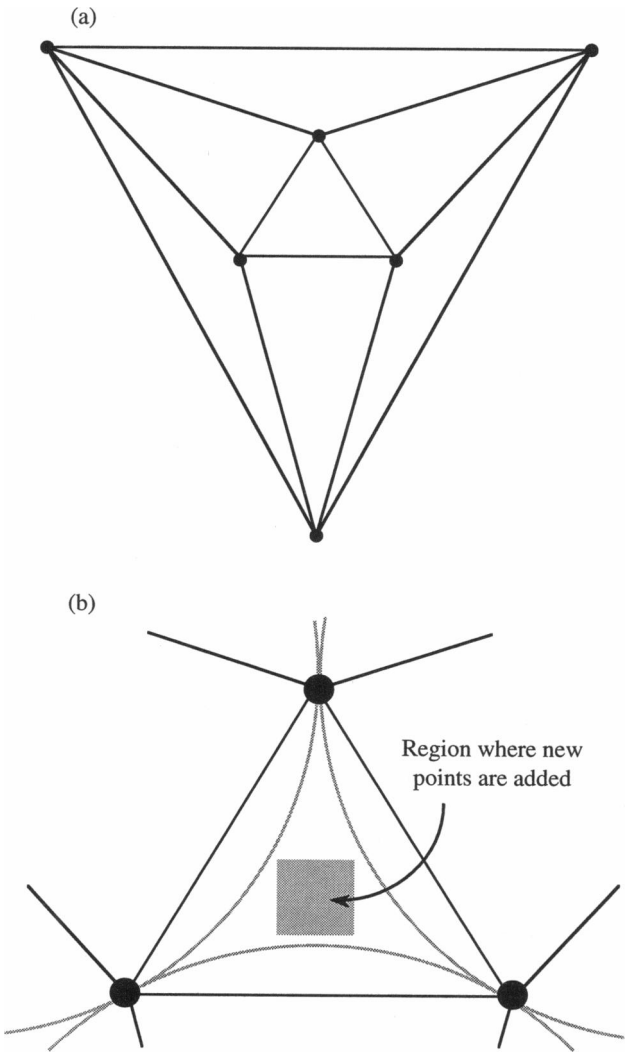

FIGURE A2 (*a*) Simple network used to initialize the incremental construction of a Delaunay triangulation; (*b*) detail of center triangle, with shaded square indicating the region where new points are added. Arcs correspond to portions of the circumcircles of the outer triangles.

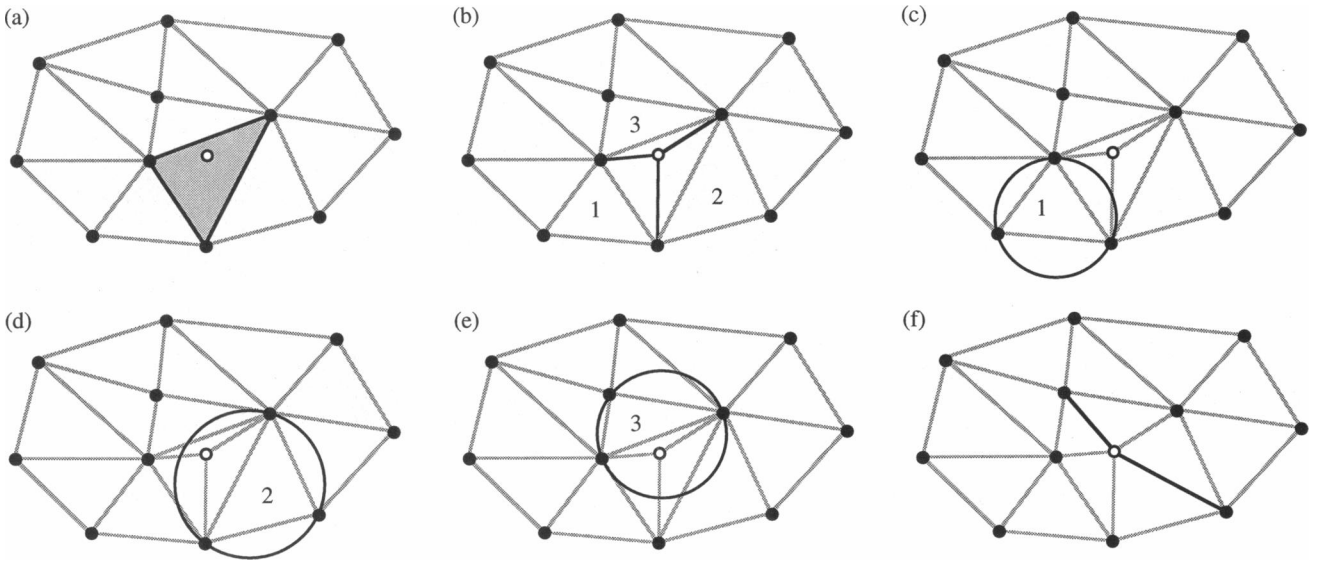

FIGURE A3 Insertion of a new point in a sample region of a valid Delaunay triangulation. (*a*) The existing triangle that contains the new point (*open circle*) is identified. (*b*) Three edges are inserted between the new point and the vertices of the surrounding triangle. (*c*) The circumcircle of neighboring triangle 1 is empty. (*d*) The circumcircle of neighbor 2 is not empty. (*e*) The circumcircle of neighbor 3 is not empty. (*f*) The edges shared with neighbors 2 and 3 are "swapped" and shown in their new positions as solid lines.

APPENDIX

Construction of a Delaunay triangulation

A Delaunay triangulation is a type of random network that has been used to model various physical systems (see e.g., Okabe et al., 1992). Given a set of generating points distributed randomly in a plane, edges may be inserted between neighboring points to create a network in which each enclosed region is a triangle. This network is called a Delaunay triangulation if and only if each triangle satisfies the "empty circumcircle criterion." By definition, the circumcircle of a triangle is "empty" if it does not enclose any of the other generating points, Fig. A1.

A Delaunay triangulation is described mathematically in terms of the relative positions of all points, edges, and triangles in the network. Arrays store the x and y coordinates for all generating points, as well as the starting point and ending point for each edge in the network. In addition to this minimal description, arrays are also maintained for each triangle to record the indices of its three associated points, edges, and neighboring triangles, which are listed in counterclockwise order. The organization of this information facilitates the network generation procedure significantly.

An incremental method is used to construct a planar Delaunay triangulation from a set of randomly distributed generating points. First, the program is initialized with a simple network that consists of 6 generating points, 12 edges, and 7 valid Delaunay triangles (Fig. A2). Additional points are inserted in a small region within the center triangle so that the circumcircles of the other six triangles do not contain any of the new points. Therefore, the same three triangles will remain on the outermost boundary of the triangulation, and all other triangles will always have three neighbors, thereby simplifying algorithms that are applied to the network. The positions of the additional points are obtained from a standard FORTRAN library function that uses a linear congruential algorithm to produce a pseudo-random sequence of real numbers, which are uniformly distributed on the interval [0,1).

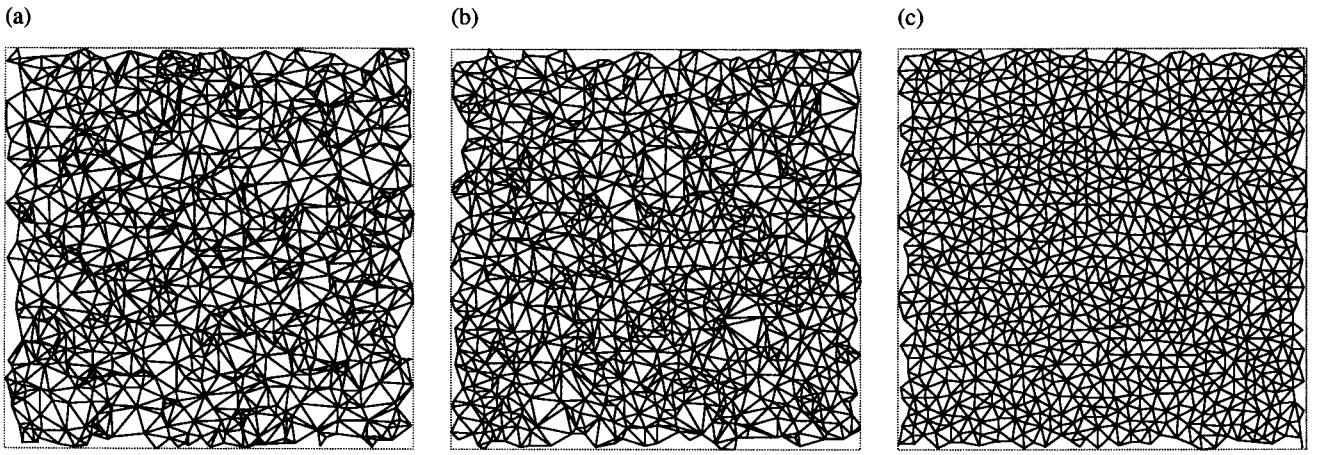

FIGURE A4 Controlling network randomness by specification of a minimum distance constraint, D_{min}, during the generation of a Delaunay triangulation. (*a*) $D_{min} = 0$, $\sigma_L = 0.491$, $\sigma_\phi = 1.362$; (*b*) $D_{min} = 0.35$, $\sigma_L = 0.401$, $\sigma_\phi = 1.198$; (*c*) $D_{min} = 0.70$, $\sigma_L = 0.218$, $\sigma_\phi = 0.851$. $N = 1000$, $B_n = 0$.

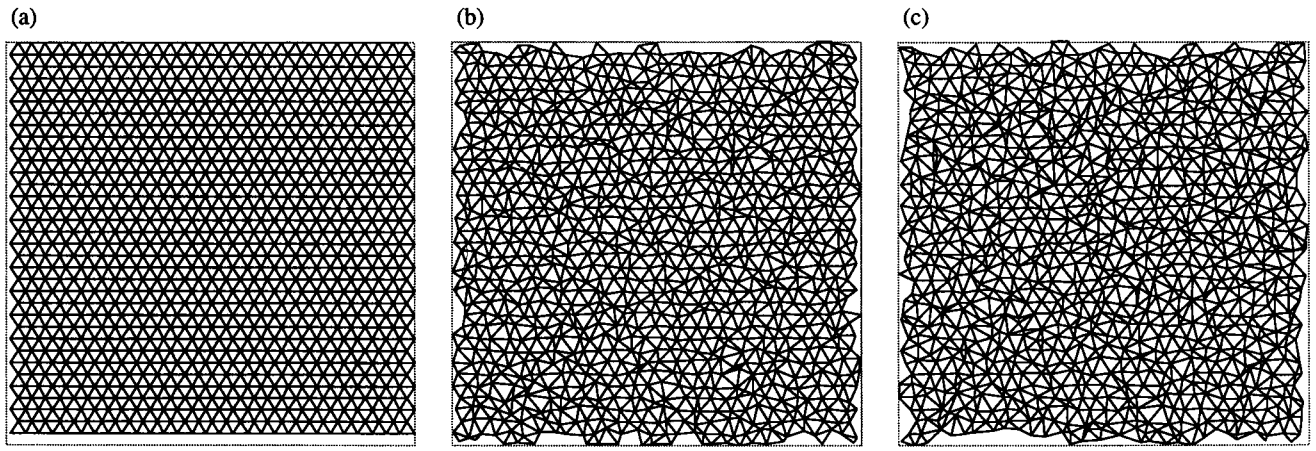

FIGURE A5 Controlling network randomness by introducing disorder in an equilateral triangular network, according to the parameter D_{dis}. (*a*) D_{dis} = 0, σ_L = 0.0, σ_ϕ = 0.0; (*b*) D_{dis} = 0.40, σ_L = 0.220, σ_ϕ = 0.364; (*c*) D_{dis} = 0.50, σ_L = 0.270, σ_ϕ = 0.750. N = 1000, B_n = 0.

Given a valid triangulation and the coordinates of a new point to be inserted, the first step is to determine which existing triangle contains the new point, Fig. A3 (*a*). Then three edges are inserted between the new point and the vertices of the surrounding triangle, Fig. A3 (*b*). The resulting network is a triangulation, but the positions of these edges will not necessarily satisfy the definition of a Delaunay triangulation.

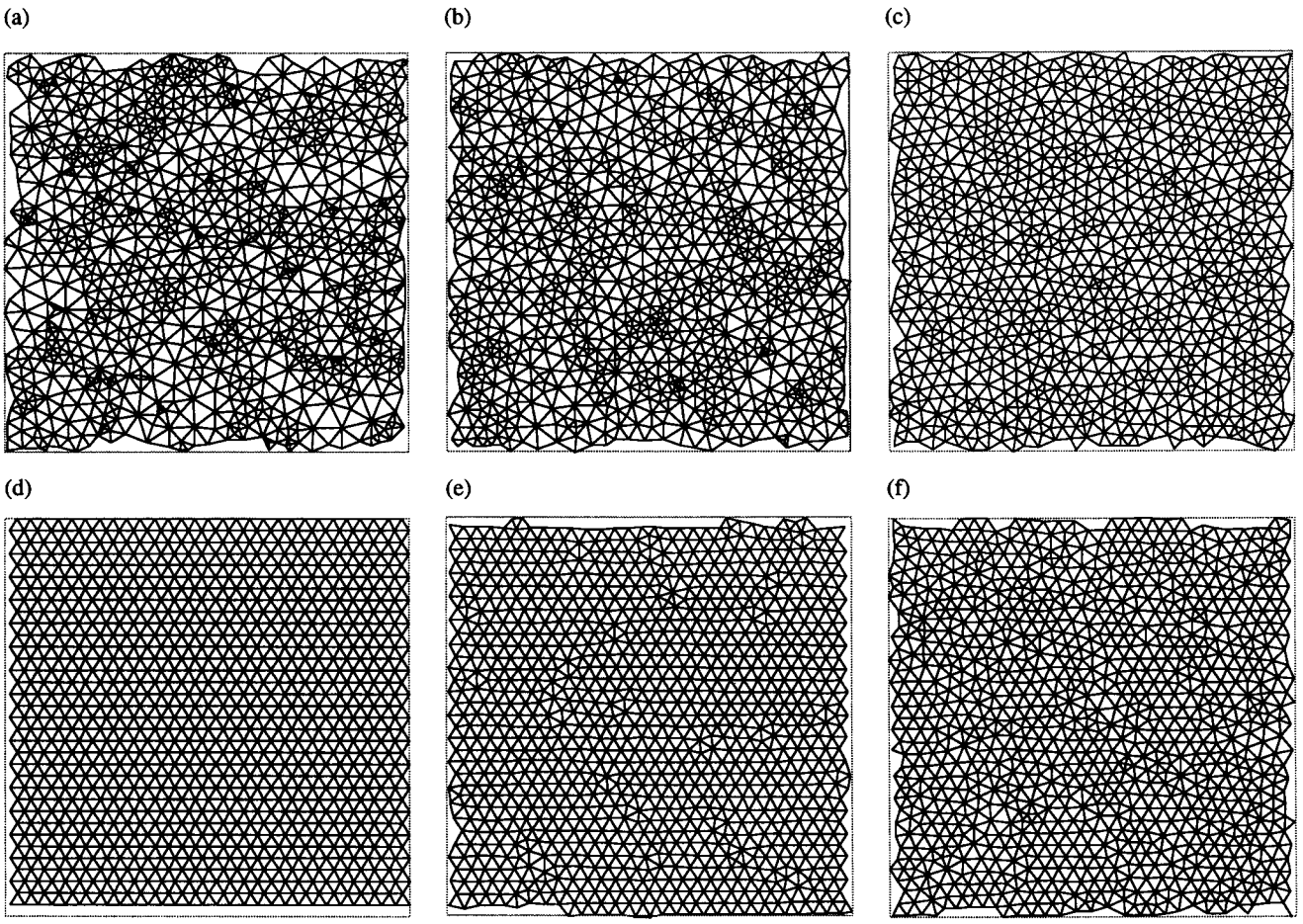

FIGURE A6 Controlling network randomness by mechanical relaxation of a Delaunay triangulation. (*a*) Relaxed form of network A2 (*a*), σ_L = 0.336, σ_ϕ = 1.365; (*b*) relaxed form of network A2 (*b*), σ_L = 0.272, σ_ϕ = 1.204; (*c*) relaxed form of network A2 (*c*), σ_L = 0.163, σ_ϕ = 0.848; (*d*) relaxed form of network A3 (*a*), σ_L = 0.0, σ_ϕ = 0.0; (*e*) relaxed form of network A3 (*b*), σ_L = 0.0633, σ_ϕ = 0.364; (*f*) relaxed form of network A3 (*c*), σ_L = 0.133, σ_ϕ = 0.747. Note the tendency for clustering in (*a*) and (*b*).

The empty circumcircle criterion is applied to the new network by testing each triangle relative to the opposite vertex in each of the three neighboring triangles. For each triangle and associated test point, this test is performed by computing the determinant of a 4 by 4 matrix. For example, consider a triangle with vertices p_i, p_j, and p_k in counterclockwise order, with Cartesian coordinates (x_i, y_i), (x_j, y_j), and (x_k, y_k), respectively. The equation of the circle passing through p_i, p_j, p_k is defined by the equation det $H = 0$, where H is the following matrix:

$$H = \begin{bmatrix} 1 & x_i & y_i & x_i^2 + y_i^2 \\ 1 & x_j & y_j & x_j^2 + y_j^2 \\ 1 & x_k & y_k & x_k^2 + y_k^2 \\ 1 & x & y & x^2 + y^2 \end{bmatrix} \quad \text{(A1)}$$

A point p with coordinates (x, y) lies inside the circle if det H < 0 and outside the circle if det H > 0. Therefore, the edges of this triangle are valid parts of a Delaunay triangulation if det H ≥ 0 for all points p. In Fig. A3, the circumcircle of neighbor 1 satisfies the empty circumcircle criterion, but the circumcircles of neighbors 2 and 3 are not empty.

If the circumcircle of a triangle does enclose a point belonging to one of its neighbors, then the shared edge between the test triangle and the neighboring triangle is swapped to the opposite diagonal of the quadrilateral formed by the two triangles, provided that the quadrilateral is not re-entrant. Two edges have been swapped in Fig. A3 (*f*). This process is repeated until all triangles in the network satisfy the empty circumcircle criterion. Then the network is a valid Delaunay triangulation, and another point may be inserted until the desired number of generating points has been used.

Controlling the randomness of a Delaunay triangulation

In a planar Delaunay triangulation, each point joins an average of six edges ($\phi = 6$). The standard deviation of edge length (σ_L) and the standard deviation of the number of edges per node (σ_ϕ) are determined by the positions of the generating points. A Delaunay triangulation may be perfectly regular, as is the case for an equilateral triangular network, having exactly six edges per vertex, with uniform edge lengths. Alternatively, a highly random distribution of generating points in the plane may produce a broad distribution of both edge lengths and number of edges per node.

Various techniques may be used to construct a Delaunay triangulation with a controlled degree of randomness. One common method involves the specification of a minimum distance, D_{min}, which must be maintained between any two generating points (Fig. A4). A new point is rejected if it lies within D_{min} of previously assigned nodes. This is analogous to placing a rigid disk with a finite radius ($D_{min}/2$) at each vertex in the triangulation. When $D_{min} = 0$, the network is considered to be completely random. As D_{min} increases, the resulting network becomes more regular until a "maximum packing configuration" is achieved, which corresponds to a maximum value for D_{min}. Network randomness may also be controlled by introducing some degree of disorder, D_{dis}, to each of the points in an equilateral triangular network (Fig. A5). Random values for the angle $[0,2\pi)$ and displacement magnitude $[0,D_{dis})$ are generated for each point. The Delaunay triangulation is then recomputed for the new set of generating points.

The randomness of a Delaunay triangulation may also be modified after the network has been constructed. If each edge is treated as a spring with some degree of initial tension or compression and the nodes on the outer boundary are fixed in their original positions, then the internal portion of the network may be "relaxed" to a state of mechanical equilibrium (Fig. A6). The final distribution of edge lengths is a function of both the initial network topology and the rest length that is defined for each spring. In this analysis, we assume a rest length of zero whenever a network is subjected to mechanical relaxation. After mechanical relaxation, there may be stresses in some or all of the springs. These stresses are neglected when the relaxed network is used as the unstressed state of the model network in further computations.

This work was supported by a predoctoral fellowship from the American Heart Association, California Affiliate (J. C. Hansen), an NSF predoctoral fellowship (J. C. Hansen), an NSF PYI Grant CMS 90–57629 (A. Hoger), and a grant from the Whitaker Foundation (A. Hoger).

REFERENCES

Arbabi, S., and M. Sahimi. 1993. Mechanics of disordered solids. I. Percolation on elastic networks with central forces. *Phys. Rev.* B47: 695–702.

Beale, P. D., and D. J. Srolovitz. 1988. Elastic fracture in random materials. *Phys. Rev. B37:5500–5507.*

Bennett, V., and D. M. Gilligan. 1993. The spectrin-based membrane skeleton and micron-scale organization of the plasma membrane. *Annu. Rev. Cell Biol.* 9:27–66.

Boal, D., U. Seifert, and J. Shillcock. 1993. Negative Poisson ratio in two-dimensional networks under tension. *Phys. Rev.* E48:4274–4283.

Boal, D. 1994. Computer simulation of a model network for the erythrocyte cytoskeleton. *Biophys. J.* 67:521–529.

Byers, T. J., and D. Branton. 1985. Visualization of the protein associations in the erythrocyte membrane skeleton. *Proc. Natl. Acad. Sci. USA.* 82:6153–6157.

Chabanel, A., K. L. P. Sung, J. Papiejko, J. T. Prchal, S.-C. Liu, and S. Chien. 1989. Viscoelastic properties of red cell membrane in hereditary elliptocytosis. *Blood.* 73:592–595.

Chasis, J. A., and N. Mohandas. 1986. Erythrocyte membrane deformability and stability: two distinct membrane properties that are independently regulated by skeletal protein associations. *J. Cell. Biol.* 103: 343–350.

Chien, S. 1977. Principles and techniques for assessing erythrocyte deformability. *Blood Cells.* 3:71–99.

Chien, S., K. Sung, R. Skalak, S. Usami, and A. Tözeren. 1978. Theoretical and experimental studies on viscoelastic properties of erythrocyte membrane. *Biophys. J.* 24:463–487.

Chien, S., and L. A. Sung. 1990. Molecular basis of red cell membrane rheology. *Biorheology* 27:327–344.

Curtin, W. A., and H. Scher. 1990. Brittle fracture in disordered materials: a spring network model. *J. Mater. Res.* 5:535–553.

Deuticke, B., R. Grebe, and C. W. M. Haest. 1990. Action of drugs on the erythrocyte membrane. *In* Blood Cell Biochemistry. J. R. Harris, editor. Plenum Press, New York. 475–529.

Discher, D. E., N. Mohandas, and E. A. Evans. 1994. Molecular maps of red cell deformation: hidden elasticity and in situ connectivity. *Science.* 266:1032–1035.

Evans, E. A. 1973. A new material concept for the red cell membrane. *Biophys. J.* 13:926–940.

Evans, E. A., and R. Skalak. 1980. Mechanics and Thermodynamics of Membranes. CRC Press, Boca Raton, Florida.

Fischer, T. M. 1992. Is the surface area of the red cell membrane skeleton locally conserved? *Biophys. J.* 61:298–305.

Fowler, V. M., and D. L. Taylor. 1980. Spectrin plus band 4.1 cross-link actin. *J. Cell Biol.* 85:361–376.

Gaydos, J. 1994. A coupled elasto-diffusion problem of integral proteins on the surface of a deformed axisymmetric erythrocyte. *In* Fundamentals of Biomedical Heat Transfer. ASME, New York. HTD-295:47–61.

Gilligan, D., and V. Bennett. 1993. The junctional complex of the membrane skeleton. *Semin. Hematol.* 30:74–83.

Grimson, M. J. 1993. Fracture of random central force networks under tension: the stretched net model of the erythrocyte membrane skeleton. *J. Phys.: Condens. Matter.* 5:4749–58.

Hochmuth, R. M., and R. E. Waugh. 1987. Erythrocyte membrane elasticity and viscosity. *Annu. Rev. Physiol.* 49:209–219.

Kozlov, M. M., and V. S. Markin. 1987. Model of red blood cell membrane skeleton: electrical and mechanical properties. *J. Theor. Biol.* 129: 439–452.

Liu, S., L. Derick, and J. Palek. 1987. Visualization of the hexagonal lattice in the erythrocyte membrane skeleton. *J. Cell Biol.* 104:527–536.

Liu, S.-C., L. H. Derick, and J. Palek. 1990. Molecular anatomy of erythrocyte membrane skeleton in health and disease. *In* Cellular and Molecular Biology of Normal and Abnormal Erythroid Membranes. C. M. Cohen and J. Palek, editors. Wiley-Liss, New York. 171–183.

Liu, S.-C., L. H. Derick, and J. Palek. 1993. Dependence of the permanent deformation of red blood cell membranes on spectrin dimer-tetramer equilibrium: implication for permanent membrane deformation of irreversibly sickled cells. *Blood.* 81:522–528.

Liu, S., P. Windisch, S. Kim, and J. Palek. 1984. Oligomeric states of spectrin in normal erythrocyte membranes: biochemical and electron microscope studies. *Cell.* 37:587–594.

McGough, A. M., and R. Josephs. 1990. On the structure of erythrocyte spectrin in partially expanded membrane skeletons. *Proc. Natl. Acad. Sci. USA.* 87:5208–5212.

Mikrut, J. M., and R. C. MacDonald. 1994. Analysis of red blood cell cytoskeleton using an atomic force microscope. *Am. Biotechnol. Lab.* 12:26.

Miyamoto, H., M. Takeuchi, H. Komizu, and A. Kusumi. 1993. Observation of microtubule and cytoskeletal structure by scanning probe microscopy. *Mol. Biol. Cell.* 4:278*a*. (Abstr.)

Mohandas, N., J. A. Chasis, and S. B. Shohet. 1983. The influence of membrane skeleton on red cell deformability, membrane properties and shape. *Semin. Hematol.* 20:225–242.

Mohandas, N., and E. Evans. 1994. Mechanical properties of the red cell membrane in relation to molecular structure and genetic defects. *Annu. Rev. Biophys. Biomol. Struct.* 23:787–818.

Nash, G. B., and W. B. Gratzer. 1993. Structural determinants of the rigidity of the red cell membrane. *Biorheology.* 30:397–407.

Ohanian, V., L. C. Wolfe, K. M. John, J. C. Pinder, and S. E. Lux. 1984. Analysis of the ternary interaction of the red cell membrane skeletal proteins spectrin, actin, and 4.1. *Biochemistry.* 23:4416–4420.

Ohno, S., N. Terada, Y. Fujii, and H. Ueda. 1994. Membrane skeleton in fresh unfixed erythrocytes as revealed by a rapid-freezing and deep-etching method. *J. Anat.* 185:415–420.

Okabe, A., B. Boots, and K. Sugihara. 1992. Spatial Tessellations: Concepts and Applications of Voronoi Diagrams. John Wiley, Chichester, England.

Ostoja-Starzewski, M., and C. Wang. 1989. Linear elasticity of planar Delaunay networks: random field characterization of effective moduli. *Acta Mechanica.* 80:61–80.

Ostoja-Starzewski, M., and C. Wang. 1990. Linear elasticity of planar Delaunay networks. Part II: Voigt and Reuss bounds, and modification for centroids. *Acta Mechanica.* 84:7–61.

Palek, J., and P. Jarolim. 1993. Clinical expression and laboratory detection of red blood cell membrane protein mutations. *Semin. Hematol.* 30: 249–283.

Parry, D. A. D., T. W. Dixon, and C. Cohen. 1992. Analysis of the three-alpha-helix motif in the spectrin superfamily of proteins. *Biophys. J.* 61:858–867.

Ralston, G. B. 1991. Temperature and pH dependence of the self-association of human spectrin. *Biochemistry.* 30:4179–4186.

Satake, M. 1985. Graph-theoretical approach to the mechanics of granular materials. *In* Continuum Models of Discrete Systems 5. A. Spencer, editor. A. A. Balkema, Rotterdam.

Saxton, M. J. 1990. The membrane skeleton of erythrocytes: a percolation model. *Biophys. J.* 57:1167–1177.

Shen, B. W. 1989. Ultrastructure and function of membrane skeleton. *In* Red Blood Cell Membranes: Structure, Function, Clinical Implications. P. Agre and J. C. Parker, editors. Marcel Dekker, New York. 261–297.

Shen, B. W., R. Josephs, and T. L. Steck. 1986. Ultrastructure of the intact skeleton of the human erythrocyte membrane. *J. Cell Biol.* 102: 997–1006.

Speicher, D. W., and V. Marchesi. 1984. Erythrocyte spectrin is comprised of many homologous triple helical segments. *Nature.* 311:177–180.

Stokke, B. T., A. Mikkelsen, and A. Elgsaeter. 1986. The human erythrocyte membrane skeleton may be an ionic gel. I. Membrane mechanochemical properties. *Eur. Biophys. J.* 13:203–218.

Svoboda, K., C. Schmidt, D. Branton, and S. Block. 1992. Conformation and elasticity of the isolated red blood cell membrane skeleton. *Biophys. J.* 63:784–793.

Ungewickell, E., and W. Gratzer. 1978. Self-association of human spectrin: a thermodynamic and kinetic study. *Eur. J. Biochem.* 88:379–385.

Ursitti, J. A., and V. M. Fowler. 1994. Immunolocalization of tropomodulin, tropomyosin, and actin in spread human erythrocyte skeletons. *J. Cell. Sci.* 107:1633–1639.

Ursitti, J. A., D. W. Pumplin, J. B. Wade, and R. J. Bloch. 1991. Ultrastructure of the human erythrocyte cytoskeleton and its attachment to the membrane. *Cell Motil. Cytoskeleton.* 19:227–243.

Ursitti, J. A., and J. B. Wade. 1993. Ultrastructure and immunocytochemistry of the isolated human erythrocyte membrane skeleton. *Cell Motil. Cytoskeleton.* 25:30–42.

Vertessy, B. G., and T. L. Steck. 1989. Elasticity of the human red cell membrane skeleton. Effects of temperature and denaturants. *Biophys. J.* 55:255–262.

Waldman, L., Y. C. Fung, and J. Covell. 1985. Transmural myocardial deformation in the canine left ventricle. *Circ. Res.* 57:152–163.

Waugh, R. E., and P. Agre. 1988. Reductions of erythrocyte membrane viscoelastic coefficients reflect spectrin deficiencies in hereditary spherocytosis. *J. Clin. Invest.* 81:133–141.

Waugh, R. E., and E. A. Evans. 1979. Thermoelasticity of red blood cell membrane. *Biophys. J.* 26:115–132.

Yan, Y., E. Winograd, A. Viel, T. Cronin, S. C. Harrison, and D. Branton. 1993. Crystal structure of the repetitive segments of spectrin. *Science.* 262:2027–2030.